Meson-resonance production in π^+p interactions at 15 GeV/c*

C. Baltay, C. V. Cautis, D. Cohen,† S. Csorna,‡ M. Kalelkar, and D. Pisello§
Columbia University, New York, New York 10027

W. D. Smith and N. Yeh
State University of New York at Binghamton, Binghamton, New York 13901

(Received 11 May 1977)

We report on a study of 15-GeV/c π^+p interactions of all topologies using the SLAC 82-in. hydrogen bubble chamber. A description is given of the automatic pattern-recognition techniques used to measure the events. Cross sections are given for meson-resonance prodcution in all topologies. Evidence is presented for a new resonance decaying to five pions. A measurement is made of the branching ratios of the g meson. A study is made of low-mass enhancements in the diffractively produced $\rho\pi$, $f\pi$, and $g\pi$ channels, and a search is made for nondiffractive production of the A_1 meson.

I. INTRODUCTION

We have made a study of π^+p interactions of all topologies using an exposure of the SLAC 82-in. hydrogen bubble chamber to a beam of 15-GeV/c π^+ mesons. We have previously published some results from the experiment.[1-6] In the present paper, we discuss meson-resonance production in the following reactions:

$$\pi^+ + p \to p + \pi^+ + \pi^+ + \pi^- , \quad (1)$$

$$\pi^+ + p \to p + \pi^+ + \pi^+ + \pi^- + \pi^0 , \quad (2)$$

$$\pi^+ + p \to p + 3\pi^+ + 2\pi^- , \quad (3)$$

$$\pi^+ + p \to p + 3\pi^+ + 2\pi^- + \pi^0 , \quad (4)$$

$$\pi^+ + p \to p + 4\pi^+ + 3\pi^- , \quad (5)$$

$$\pi^+ + p \to p + 4\pi^+ + 3\pi^- + \pi^0 . \quad (6)$$

Section II is a description of the experimental procedure. In Sec. III, we present general features of the interaction, including topological and reaction cross sections. We also discuss resonance production in various channels. Section IV reports a measurement of the branching ratios of the g meson. In Sec. V, we present a search for some high-mass resonances previously claimed in the literature. The production of A enhancements in $\rho\pi$, $f\pi$, and $g\pi$ channels is discussed in Sec. VI.

II. EXPERIMENTAL PROCEDURE

A. The exposure

The experiment was performed at SLAC using the 15-GeV/c secondary hadron beam. An rf separator was used to select π^+ mesons, which were then incident on the 82-in. bubble chamber filled with liquid hydrogen. On the average, there were 12.2 incoming π^+ beam particles for each expansion of the bubble chamber. A total of 866 000 pictures was taken during three separate runs at SLAC.[7] Using a Čerenkov counter, the beam contamination due to K mesons and protons was estimated to be $(0.1 \pm 0.1)\%$.

Optical constants were determined by making many measurements of 15 fiducial marks scratched on the bottom of the front glass, and fitting to their positions as found from a survey.[8] Distortion terms up to third order were needed to obtain acceptable fits. The final set of optical constants used in the experiment yielded an rms of 60 μm in space for the fiducials. There were some variations in the constants from run to run. As discussed in Sec. III D, the average point setting error was 100 μm in space.

In order to parametrize the magnetic field, a polynomial fit was made to known values of the field intensity at numerous points in the chamber.[9,10] An rms deviation of 13 G was obtained. The magnitude of the field in the center of the chamber was 15.5 kG.[11]

To determine the liquid-hydrogen density, measurements were made of the length of muon tracks coming from the decay of pions at rest. The hydrogen density was calculated to be 0.0636 ± 0.0006 g/cm^3 to reproduce the known muon momentum.

B. Scanning of events

A total scan of the exposure was performed to obtain the topology and location of each event. Primary interactions were scanned for in a fiducial volume with a length of 118.37 cm along the beam direction. No restrictions were imposed in the direction perpendicular to the beam. The vertex points of all primary reactions were measured along

TABLE I. Topological cross sections and scan efficiencies.

Topology	Scan efficiency (%)	Cross section (mb)
2	89.2±1.4	8.16 ±0.16
4	94.8±1.4	9.26 ±0.18
6	94.5±1.9	5.06 ±0.12
8	93.8±2.3	1.33 ±0.04
10	83.2±2.5	0.21 ±0.01
12	73±7	0.024±0.003
14	73±7	0.003±0.001
Total	92.6±1.4	24.05 ±0.28

with a code indicating the topology of the cited event.

The scanners also flagged tracks that were identifiable as protons from ionization. (The accuracy of this identification is discussed later.) The scanners made this selection of a proton in approximately half the events.

Vertices of vees pointing to primaries, and all obvious neutron interaction points, were also measured. No fiducial volume was imposed for vees and neutron scatters. Kinks on primary prongs were measured with codes to indicate the charge of the decaying track. Finally, as an aid to the automatic measuring procedure used in the experiment, the endpoints of all tracks less than 10 cm long were measured.

About 10% of the exposure was scanned a second time to evaluate scan efficiencies. These are given in Table I as functions of topology.

C. Measurement of events

1. On-line HPD processing

All the scanned events were measured on the Hough-Powell device (HPD), a device that used a flying spot of light to scan a picture in a raster pattern.[12] The source of light was a mercury arc lamp, from which two rays were drawn, which were eventually used for two perpendicular scans of a picture. Each ray of light fell upon a 1-mm fixed fiber. The spot was formed by the crossing of the fixed fiber and one of eight curved fibers on a disk rotating at 5400 rpm. The spot moved in space as the disk rotated, and this motion constituted the scan line. The emerging spot was then split in two, with one beam traveling to a grating and photomultiplier to mark the position of the spot in the scan line. The other beam was conducted onto the film itself, which was vacuum clamped to a platen attached to a stage. A photomultiplier and discriminator determined the presence or absence of a bubble from the intensity of the light passing through the film. The diameter of the spot was about 20 μm.

In the so-called normal scan, the motion of the spot in a single scan line was perpendicular to the beam track direction. To scan the entire picture, the stage was moved hydraulically at a speed of about 1 cm/sec, resulting in a scan line spacing of 42 μm. The stage position was determined using a grating and photomultiplier (with a fixed spot of light) similar to that used to locate the flying spot in the scan line. Two coordinates were thus obtained for every position of the spot on the film. The least count of the coordinates was 2 μm on film.

Tracks perpendicular to the beam track direction were inadequately digitized in the normal scan. An "abnormal" scan for every picture was therefore also performed using the second ray of light from the mercury arc lamp. A prism was used to conduct the abnormal spot onto the film parallel to the beam direction. The stage was then moved perpendicular to the plane of the film to allow a complete scan.

The HPD was operated in an automatic mode, under the control of a "track following program" (TFP) written for the Columbia University 360/91 computer.[13,14] A list of frame numbers for all the scanned events was supplied to the program, along with the coordinates of the interaction-vertex points. The HPD measured only those frames having at least one primary event, thereby saving a large amount of time. (About 30% of the pictures were without events.) The normal scan was performed first, providing (x,y) coordinates of approximately 45 000 digitizings to the TFP. The main purpose of the TFP was to separate digitizings belonging to different tracks. Circle fits were made to clusters of digitizings to determine if they belonged to a common track. For each segment, the circle was extrapolated to define a "road" in which digitizings from subsequent scan lines would be expected to fall. Digitizings lying within such roads were associated with the corresponding tracks, while others were used to initialize new tracks. Coordinates of associated digitizings were averaged once every 15 scan lines, and only these "average points" were retained. The separation between average points was about 1.25 cm in space.

Digitizings from the abnormal scan, typically about 25 000, were track followed in the same way as for the normal scan. The track following procedure itself made no use of the scan information.

Upon completion of track following, there were some 250 track segments and 2300 average points on each frame. Use of the scanned vertex coordinates was now made to reduce the actual output. Track segments were fitted to circles, which were

examined to see if they passed or extrapolated through the vertices within a large tolerance. Tracks which were clearly unassociated with events were eliminated. The final output from TFP, consisting of about 26 track segments and 540 average points, was written on magnetic tape. The complete scan of a frame in one view took about 13 seconds. The actual average weekly measurement rate achieved was 12 rolls of film, which comprised over 10 000 events in three views.

2. *Single-view off-line processing*

Numerous checks were performed off-line on the HPD output. In many instances there was more than one track segment corresponding to a single physical track. Such multiplicities occurred because TFP broke up tracks in regions confused by crossing tracks. In addition, tracks were frequently found partially in the normal scan and the rest in the abnormal scan.

Linking of broken tracks and merging of tracks from the two scans were performed. Two tracks that were candidates for a link were extrapolated to a common point, and their lateral deviation there was required to be less than some tolerance. In addition, the angle between the two segments was required to be small, and finally a cut was imposed on the rms deviation of a circle fit to the combined track. This last test was used also to merge overlapping tracks from the two scans. No tracks, however, were allowed to link through a scanned vertex. This was done to ensure that forward prongs with beamlike curvature were not linked to the incoming beam track. Upon completion of the link-merge phase of processing, there were typically 12 tracks and 400 average points per frame.[15]

3. *Event finding*

In the next phase of processing, it was desired to write a measurement tape consisting of points in three views for all tracks of all events. To do this, it was necessary to match the tracks among the three views, associate each match with a scanned event, and finally determine, for each event, which of the associated matches actually corresponded to prongs of the interaction.[7]

Input to event finding consisted of the link-merge data for those frames where all three views had been successfully processed by the HPD. Two-view matching of tracks was then initiated. For a given pair of views, matching was attempted between every track of the first view and every track of the second. The following tests were made:

a. The two tracks had to have the same sign of charge.

b. They had to have comparable lengths.

c. If both tracks passed through the same scanned vertex point, they were required to be on the same side of the vertex, i.e., both above or both below. This was necessary to prevent a forward beamlike prong in one view from matching with the incoming beam in the other. This test was not applied to sideways tracks.

d. First-order optics was used to obtain corresponding points for the first, middle, and last points in view i. A line was generated through each of these points parallel to the intercamera direction, and a calculation was made of the intersection of this line with the circle or straight line fit to the track in view j. The three pairs of corresponding points thus obtained were used to derive three space points, which were required to lie on a helix. In particular, the dip angle computed from the first two points was required to be consistent with the dip angle computed from the last two.

A pair of tracks satisfying all these tests was categorized as a two-view match. Six space points were calculated for each match. This matching procedure was repeated for each of the three pairs of views. Three-view matching was then performed for each two-view match. The six space points from the latter were projected into the third view and a computation was made of the rms deviation of these points from the circle or straight-line fits to every track in the third view. Tracks for which the rms exceeded 0.3 cm were discarded; of the remainder, the track which provided the lowest rms was accepted as the matching track in the third view. Each set of matching tracks was then associated with that scanned event whose vertex was closest to the track in three dimensions.

The final step in event finding was to decide, for each event, which of the associated three-dimensional tracks actually corresponded to prongs of the interaction. It was known from the scan information how many positive and negative tracks comprised the event. The event was obtained by selecting the requisite number of tracks of each charge passing most closely through the vertex in three dimensions. If an insufficient number of tracks was available, the event was categorized as lost.

About 80% of the events were found by this procedure. A study of the losses indicated that 90% of these contained only one lost track. The lost tracks were frequently obscured in one or more views by other tracks partially overlapping them. All the lost events were remeasured on the HPD, using a different version of the track following program, concentrating on the problem of overlapping tracks in the vicinity of a vertex. After

two passes through the HPD, over 90% of the events were found.

D. Geometrical reconstruction

Reconstruction of tracks was performed using the geometry program TVGP.[16] The standard version of this program had been coded to accept a point-setting error, then propagate it into errors on momenta and angles when the space curve was fitted. A study indicated that HPD tracks could not be adequately described by a single point setting error. The actual setting error depended on track angle, curvature, and number of scan lines per average point. A new technique was used to derive the correct setting error. After completing the space curve fit to a track, TVGP calculated the rms deviation of the measured points from the curve. This value was chosen as a representation of the effective point-setting error and was used to compute the measurement contribution to the error matrix. The setting error thus varied from track to track. The average value was 5 μm on film or about 100 μm in space. For most tracks there were 40 measured points in each view.

During the HPD measurements, tracks could not be followed by the program all the way to the interaction vertex. Especially for the high multiplicity events, where many prongs converged at the vertex, the program had to close out some of the tracks several cm before reaching the vertex. A program was written to intersect the tracks of an event by using the TVGP parameters. This intersection point was projected onto each track, and the TVGP parameters at the measured beginning points were swum to the projected vertex points.[11]

A sample of noninteracting beam tracks was measured on the HPD and reconstructed in TVGP. A scatter plot of the momentum and azimuthal angle versus lateral position in the chamber displayed a clear linear correlation for both. A least-squares fit was performed, and the resulting correlation functions were used to develop a beam-averaging scheme that reduced errors on beam-track measurements considerably. The fractional error on the beam-track momentum was typically well below 1%.

A study of the HPD output indicated that 10% of the events contained a track that was not truly a prong of the interaction. Most of these fake tracks were determined to be portions of noninteracting beam tracks that lay near the scanned vertex. Checks were made on the TVGP output to detect these fake events. Tracks not passing through the calculated intersection point within a tight tolerance were recognized as fakes. Events were also considered fakes if the total outgoing longitudinal momentum was more than four standard deviations greater than the incoming beam momentum. These criteria successfully detected $(80 \pm 5)\%$ of the fakes.

A check was made of the HPD resolution and magnetic field normalization by calculating the effective mass of all vees measured by the HPD. The mass distribution of the vees interpreted as K^0's is shown in the region of the K^0 mass in Fig.

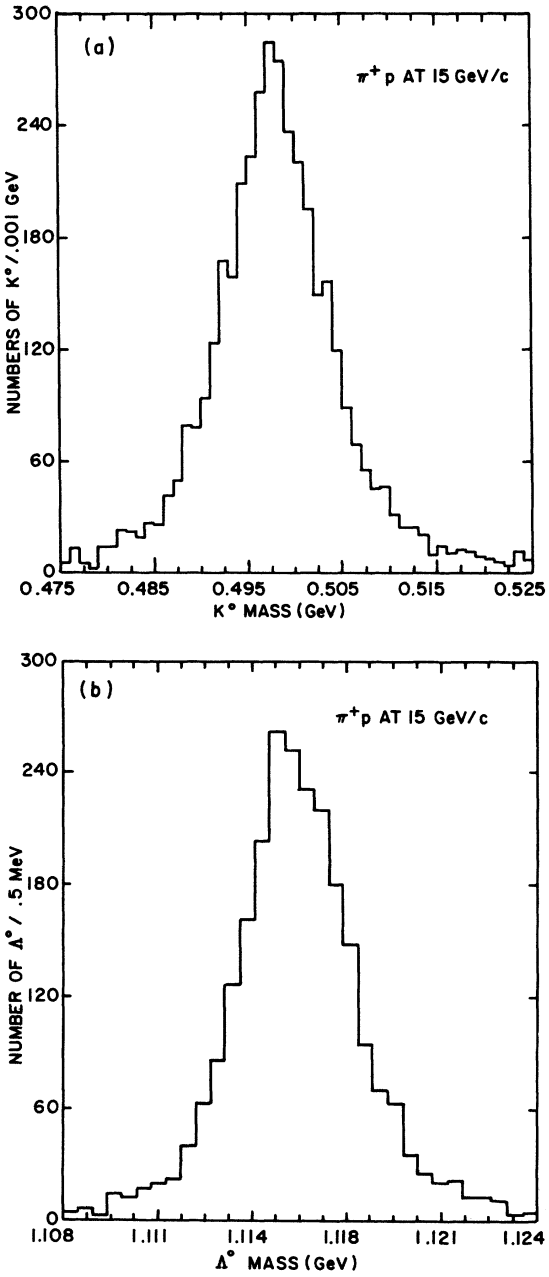

FIG. 1. Effective-mass distribution of vees interpreted as (a) K^0's, (b) Λ's.

1(a), and the corresponding distribution for Λ's is shown in Fig. 1(b). The central values of the mass plots reproduce the known K and Λ masses to within 0.5 MeV. Mass resolutions are 12 MeV full width at half maximum (FWHM) for the K and 4 MeV FWHM for the Λ.

E. Kinematic fitting and event selection

A total of 520 000 events successfully passed through all of our selection criteria and were submitted to the program SQUAW for kinematic fitting.[17] Table II lists the numbers of events by topology along with the corresponding microbarn equivalents. The overall microbarn equivalent was determined using the pion flux, fiducial volume, liquid-hydrogen density, and beam attenuation. Corrections were made for scan efficiencies and losses at each stage in the HPD measurement and data reduction.

For each event nonstrange fits were attempted in SQUAW. For the four-prong events, fits were tried to the following hypotheses:

$$\pi^+p \to p\pi^+\pi^+\pi^-, \tag{1}$$

$$\pi^+p \to p\pi^+\pi^+\pi^-\pi^0, \tag{2}$$

$$\pi^+p \to n\pi^+\pi^+\pi^+\pi^-. \tag{2a}$$

Fits for the other topologies were analogous to these.

It was found that track-permutation ambiguities for the four-constraint (4C) fits corresponding to reaction (1) were low for all topologies. (For the four-prong events, about 3% of the 4C fits were ambiguous.) However, the 1C fits corresponding to reactions (2) and (2a) were highly ambiguous. About 35% of the four-prong events making 1C fits were ambiguous either between reactions (2) and (2a), or in the assignment of the proton among the positive tracks.

To reduce fit ambiguities, it was decided to make use of the proton choice made by the scanners. In order to check the accuracy of the scanner proton selection, a sample of unambiguous 4C events with χ^2 less than 7.0 was examined. The scanners made a proton choice in 83% of these events. When a choice was made, it agreed with the proton assignment of the 4C fit in over 99% of the cases. A study of the momentum dependence of this reliability indicated that up to about 1.4 GeV/c the accuracy of the scanner choice was over 95%. To investigate the possibility that the scanners were selecting protons on events that did not actually contain protons, a sample of tracks with momenta less than 1.2 GeV/c was examined carefully on the scan table. Relative ionization was used

TABLE II. Measured events and microbarn equivalents.

Topology	Measured events	Events/μb
2	193 115	25.27 ± 0.53
4	214 025	23.19 ± 0.45
6	93 082	18.43 ± 0.44
8	17 819	13.50 ± 0.42
10	1 602	7.63 ± 0.41
12	65	2.71 ± 0.48

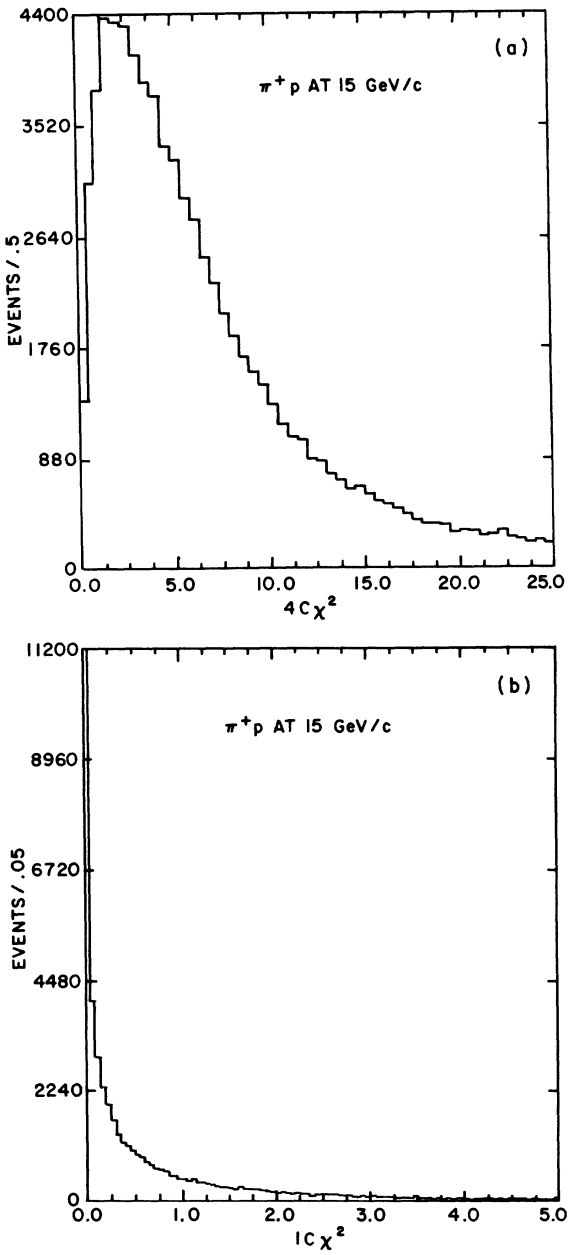

FIG. 2. χ^2 distribution for (a) 4C fits, (b) 1C fits.

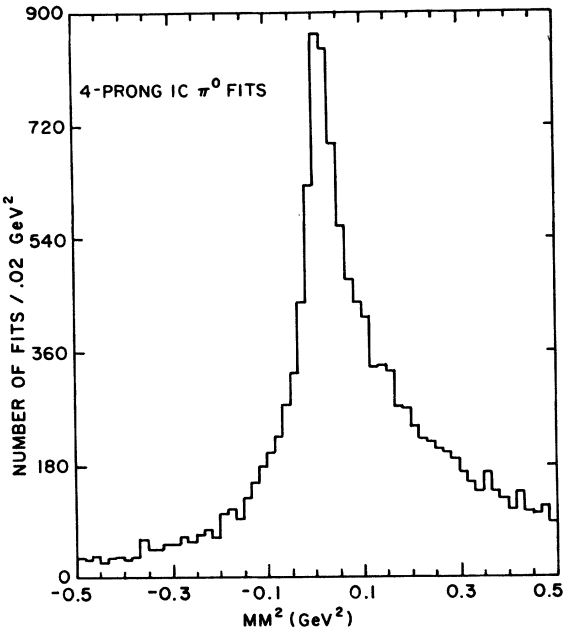

FIG. 3. Distribution of missing mass squared for four-prong 1C fits.

to isolate pions. It was found that less than 1% of these had been misidentified as protons by the scanners.

The event sample of 4C fits was selected by imposing a cut of 30.0 on the χ^2 for the fit. Events suffering a single constraint reduction due to a very short track were also accepted if the χ^2 was less than 30.0. Figure 2(a) shows the χ^2 distribution. Whenever fit ambiguities occurred, that fit was accepted whose proton track agreed with the scanner selection, provided the proton momentum was less than 1.2 GeV/c. If no scanner selection had been made, the fit with the lowest χ^2 was accepted. A check of this procedure was made on the scan table for a subsample of these events, and it was estimated that the fit with the lowest χ^2 was the correct one in about 80% of the residual ambiguous events. The fraction of fake fits in the final sample was estimated to be no more than 0.5%.

To select the 1C π^0 sample, a cut of 5.0 on the χ^2 was used to define a fit candidate. Figure 2(b) shows the distribution of the χ^2. All 1C fits were discarded for an event if an acceptable 4C fit had been achieved. Next, if a scanner selection had been made, and the momentum of the track cited as proton was less than 1.2 GeV/c, the fit was required to agree with the scanner choice. About a quarter of the events were still ambiguous after this procedure.

The next step was to examine missing mass squared distributions for the 1C candidates: Figure 3 shows this distribution for the four-prong candidates. It was decided to impose a cut on the missing mass in order to reduce the substantial contamination from multiple π^0 events. For the four-prong events, the missing mass squared for π^0 fits was required to lie between −0.17 and 0.17 GeV^2. Table III shows the cuts used for both the π^0 and neutron fits as functions of topology. It was estimated that (15 ± 5)% of the events surviving the cuts represented contamination from multiple π^0 events, while (12 ± 4)% of true π^0 events had been lost by the cuts.

After the application of all these selection criteria, 17% of the 1C fits were still ambiguous. In order to keep the final π^0 event sample as free of fake fits as possible, it was decided to accept only the unique 1C fits for analysis. Table IV shows the numbers of unique π^0 fits obtained for each topology.

TABLE III. Cuts on missing-mass squared for 1C fits.

Topology	π^0 fits (GeV^2)	Neutron fits (GeV^2)
2	−0.23, 0.23	0.00, 1.80
4	−0.17, 0.17	0.20, 1.60
6	−0.13, 0.13	0.40, 1.40
8	−0.10, 0.10	0.56, 1.24
10	−0.08, 0.08	0.66, 1.14

TABLE IV. Fitted events and cross sections.

Reaction	Events	Cross section (μb)
$\pi^+ p \to p\pi^+\pi^+\pi^-$	25991	1132 ± 42
$\pi^+ p \to p\pi^+\pi^+\pi^-\pi^0$	19531	1005 ± 77
$\pi^+ p \to p3\pi^+2\pi^-$	7688	395 ± 16
$\pi^+ p \to p3\pi^+2\pi^-\pi^0$	11316	777 ± 62
$\pi^+ p \to p4\pi^+3\pi^-$	1733	114 ± 7
$\pi^+ p \to p4\pi^+3\pi^-\pi^0$	2440	244 ± 21
$\pi^+ p \to p5\pi^+4\pi^-$	196	21 ± 2
$\pi^+ p \to p5\pi^+4\pi^-\pi^0$	254	49 ± 6
$\pi^+ p \to p6\pi^+5\pi^-$	8	2.3 ± 0.9
$\pi^+ p \to p6\pi^+5\pi^-\pi^0$	17	10 ± 3

III. GENERAL FEATURES OF THE INTERACTION

A. Topological and reaction cross sections

Topological cross sections were calculated for all the topologies observed and are given in Table I. The two-prong cross section includes a correction (0.52 ± 0.02 mb) for events not detected be-

cause of very low momentum transfer to the outgoing proton. The errors on the cross sections include contributions from the uncertainties in our knowledge of the pion flux, hydrogen density, and scan efficiency, in addition to the statistical error. We obtain a total cross section of 24.05 ± 0.28 mb, which is in very good agreement with counter measurements.[18]

In Table IV we list the cross sections for the reactions corresponding to the 4C and 1C π^0 fits performed in this experiment. The cross sections were determined using the numbers of fitted events and the microbarn equivalent for each topology, and correcting for fake events not detected after TVGP and for fake fits contaminating the sample. (The 1C fits had a non-negligible contamination from multi-π^0 events.) The 1C fits were also further corrected for losses due to the missing mass cuts and the requirement of a unique fit. The errors given for the cross sections include the statistical error, the uncertainties in the microbarn equivalent and in each of the corrections made.

B. Meson-resonance production

1. $\pi^+ p \to p\pi^+\pi^+\pi^-$

A total of 25 991 events satisfied all our selection criteria for the reaction

$$\pi^+ p \to p\pi^+\pi^+\pi^-. \qquad (1)$$

Figure 4 shows the effective-mass distribution

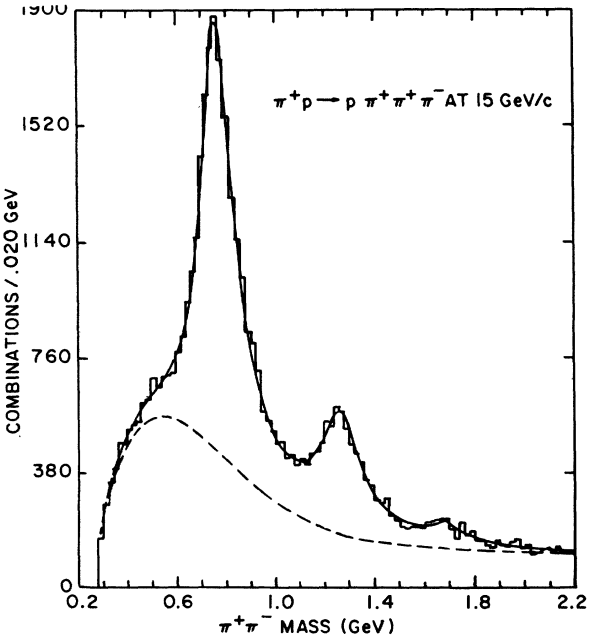

FIG. 4. $\pi^+\pi^-$ mass distribution from reaction (1).

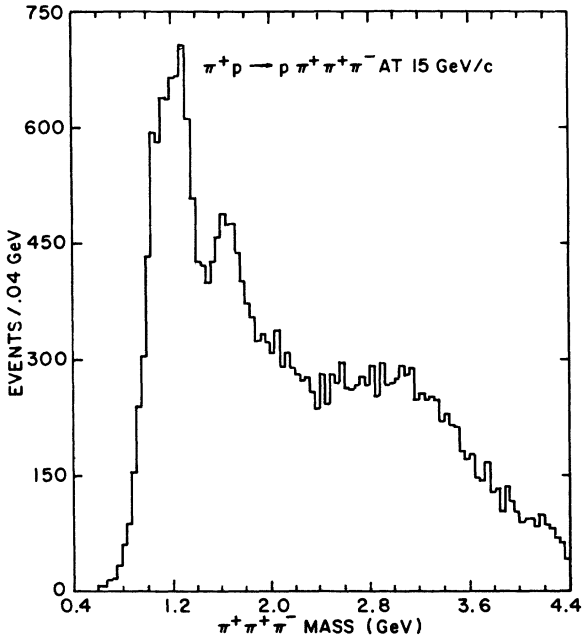

FIG. 5. $\pi^+\pi^+\pi^-$ mass distribution from reaction (1).

of the $\pi^+\pi^-$ system, with two combinations per event. There is clear production of the ρ^0, f^0, and g^0 mesons. The solid curve is a fit to the data, using a smooth background polynomial and Breit-Wigner shapes multiplied by phase space for the resonances. The best fit to the spectrum yielded the following values for the masses and widths of the resonances:

ρ: $M = 767 \pm 2$ MeV, $\Gamma = 159 \pm 7$ MeV,

f: $M = 1260 \pm 4$ MeV, $\Gamma = 199 \pm 20$ MeV,

g: $M = 1679 \pm 11$ MeV, $\Gamma = 116 \pm 30$ MeV,

Cross sections for the production of these resonances in reaction (1) were computed using the numbers of events in the resonances and the microbarn equivalent corrected as described in the previous section. Table V lists the cross sections. All errors given on resonance cross sections include the effect of the uncertainty in the resonance width, the uncertainty in the shape of the background, the statistical error, and the uncertainty in the corrected microbarn equivalent.

For all fits to mass distributions reported in this paper, we have used a polynomial background and a simple nonrelativistic S-wave Breit-Wigner shape for a resonance. The mass and width of the resonance were allowed to vary in order to obtain the best fit to the distribution. In all cases, the χ^2 of the final fit was less than $1\frac{1}{2}$ times the number of degrees of freedom, and in most cases, it was much less. Errors on the mass and width

TABLE V. Resonance production cross section. The "events" column indicates the amount of resonance production in a particular final state. An event with two ρ^0's, for example, would contribute two entries to this column.

Channel	Events	Cross section (μb)
1. $\pi^+p \to p\pi^+\pi^+\pi^-$		
$p\pi^+\rho^0$, $\rho^0 \to \pi^+\pi^-$	16 267	708 ± 35
$p\pi^+f^0$, $f^0 \to \pi^+\pi^-$	4 970	216 ± 23
$p\pi^+g^0$, $g^0 \to \pi^+\pi^-$	476	20.7 ± 5.4
2. $\pi^+p \to p\pi^+\pi^+\pi^-\pi^0$		
$p\pi^+\pi^0\rho^0$, $\rho^0 \to \pi^+\pi^-$	4 853	250 ± 34
$p\pi^+\pi^0f^0$, $f^0 \to \pi^+\pi^-$	603	31 ± 13
$p\pi^+\pi^-\rho^+$, $\rho^+ \to \pi^+\pi^0$	4 012	206 ± 19
$p\pi^+\pi^+\rho^-$, $\rho^- \to \pi^-\pi^0$	1 243	64 ± 16
$p\pi^+\eta$, $\eta \to \pi^+\pi^-\pi^0$	143	7.4 ± 1.2
$p\pi^+\omega$, $\omega \to \pi^+\pi^-\pi^0$	900	46.3 ± 4.9
$p\pi^+A_2^0$, $A_2^0 \to \pi^+\pi^-\pi^0$	659	33.9 ± 6.8
$p\pi^0A_2^+$, $A_2^+ \to \pi^+\pi^+\pi^-$	438	22.5 ± 4.4
pB^+, $B^+ \to \pi^+\pi^+\pi^-\pi^0$	225	11.6 ± 4.3
pA_2^+, $A_2^+ \to \eta\pi^+$, $\eta \to \pi^+\pi^-\pi^0$	83	4.3 ± 1.0
pg^+, $g^+ \to \pi^+\pi^+\pi^-\pi^0$	177	9.1 ± 2.6
3. $\pi^+p \to p3\pi^+2\pi^-$		
$p2\pi^+\pi^-\rho^0$, $\rho \to \pi^+\pi^-$	6 145	316 ± 25
$p2\pi^+\pi^-f^0$, $f^0 \to \pi^+\pi^-$	887	45.6 ± 12.9
$p\pi^+\pi^-A_2^+$, $A_2^+ \to \pi^+\pi^+\pi^-$	1 049	53.9 ± 8.5
$p2\pi^+A_2^-$, $A_2^- \to \pi^+\pi^-\pi^-$	375	19.3 ± 3.1
$p(2340)^+$	142	7.3 ± 1.7
4. $\pi^+p \to p3\pi^+2\pi^-\pi^0$		
$p2\pi^+\pi^-\pi^0\rho^0$, $\rho^0 \to \pi^+\pi^-$	3 991	274 ± 40
$p2\pi^+\pi^-\pi^0f^0$, $f^0 \to \pi^+\pi^-$	432	30 ± 18
$p2\pi^+2\pi^-\rho^+$, $\rho^+ \to \pi^+\pi^0$	962	66 ± 24
$p3\pi^+\pi^-\rho^-$, $\rho^- \to \pi^-\pi^0$	529	36 ± 16
$p2\pi^+\pi^-\eta$, $\eta \to \pi^+\pi^-\pi^0$	239	16.4 ± 2.4
$p2\pi^+\pi^-\omega$, $\omega \to \pi^+\pi^-\pi^0$	1 115	77 ± 9
$p2\pi^+\pi^-A_2^0$, $A_2^0 \to \pi^+\pi^-\pi^0$	330	23 ± 9
$p\pi^+\pi^-\pi^0A_2^+$, $A_2^+ \to \pi^+\pi^+\pi^-$	296	20 ± 11
$p2\pi^+\pi^0A_2^-$, $A_2^- \to \pi^+\pi^-\pi^-$	78	5.4 ± 6.3
5. $\pi^+p \to p4\pi^+3\pi^-$		
$p3\pi^+2\pi^-\rho^0$, $\rho^0 \to \pi^+\pi^-$	1 166	76 ± 15
$p3\pi^+2\pi^-f^0$, $f^0 \to \pi^+\pi^-$	95% C.L.	< 3.9
$p2\pi^+2\pi^-A_2^+$, $A_2^+ \to \pi^+\pi^+\pi^-$	95% C.L.	< 6.8
$p3\pi^+\pi^-A_2^-$, $A_2^- \to \pi^+\pi^-\pi^-$	95% C.L.	< 5.5
6. $\pi^+p \to p4\pi^+3\pi^-\pi^0$		
$p3\pi^+2\pi^-\pi^0\rho^0$, $\rho^0 \to \pi^+\pi^-$	1 578	158 ± 18
$p3\pi^+2\pi^-\pi^0f^0$, $f^0 \to \pi^+\pi^-$	95% C.L.	< 5.6
$p3\pi^+3\pi^-\rho^+$, $\rho^+ \to \pi^+\pi^0$	320	32 ± 9
$p4\pi^+2\pi^-\rho^-$, $\rho^- \to \pi^-\pi^0$	146	15 ± 6
$p3\pi^+2\pi^-\eta$, $\eta \to \pi^+\pi^-\pi^0$	91	9.1 ± 3.3
$p3\pi^+2\pi^-\omega$, $\omega \to \pi^+\pi^-\pi^0$	221	22 ± 6
$p3\pi^+2\pi^-A_2^0$, $A_2^0 \to \pi^+\pi^-\pi^0$	95% C.L.	< 10
$p2\pi^+2\pi^-\pi^0A_2^+$, $A_2^+ \to \pi^+\pi^+\pi^-$	95% C.L.	< 12
$p3\pi^+\pi^-\pi^0A_2^-$, $A_2^- \to \pi^+\pi^-\pi^-$	95% C.L.	< 9.5

were determined by noting what range of these parameters caused an increase of one in the χ^2. For the background, we used the lowest-order polynomial needed for an acceptable fit. In no case was this higher than fourth order.

The sum of the cross sections for ρ, f, and g production in reaction (1) is 945 ± 42 μb. This implies that reaction (1) proceeds by ρ, f, or g production $(83 \pm 5)\%$ of the time. The g meson is discussed in greater detail in Sec. IV.

Figure 5 shows the effective mass of the $\pi^+\pi^+\pi^-$ system. There is a broad peak in the region of the A_1 and A_2 mesons, as well as a very clear signal for the A_3. The A mesons are discussed in Sec. VI and Ref. 31.

2. $\pi^+p \to p\pi^+\pi^+\pi^-\pi^0$

A total of 19 531 events satisfied our selection criteria for the reaction

$$\pi^+p \to p\pi^+\pi^+\pi^-\pi^0. \quad (2)$$

The $\pi^+\pi^-$, $\pi^+\pi^0$, and $\pi^-\pi^0$ mass distributions are shown in Figs. 6–8, respectively. The ρ meson is present in all three channels, and cross sections for its production are given in Table V. The $\pi^+\pi^-$ plot also shows a small signal for the f meson while there is no clear evidence for the g meson in any of the distributions.

Figure 9 shows the $\pi^+\pi^-\pi^0$ mass distribution. We observe prominent signals for the η, ω, and A_2

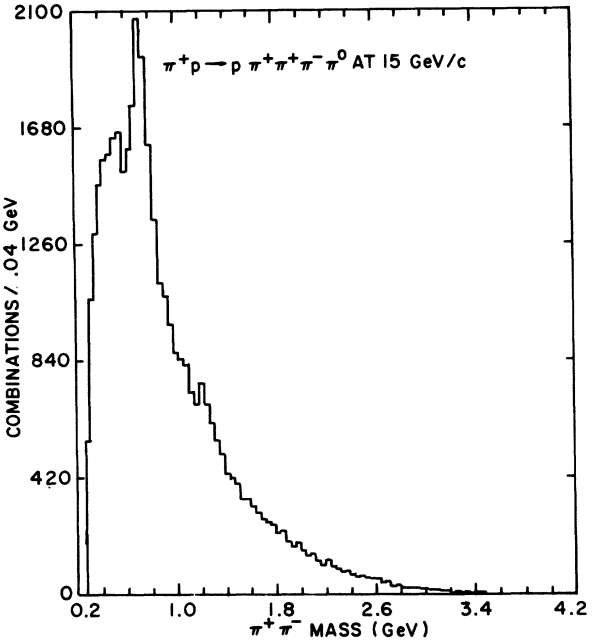

FIG. 6. $\pi^+\pi^-$ mass distribution from reaction (2).

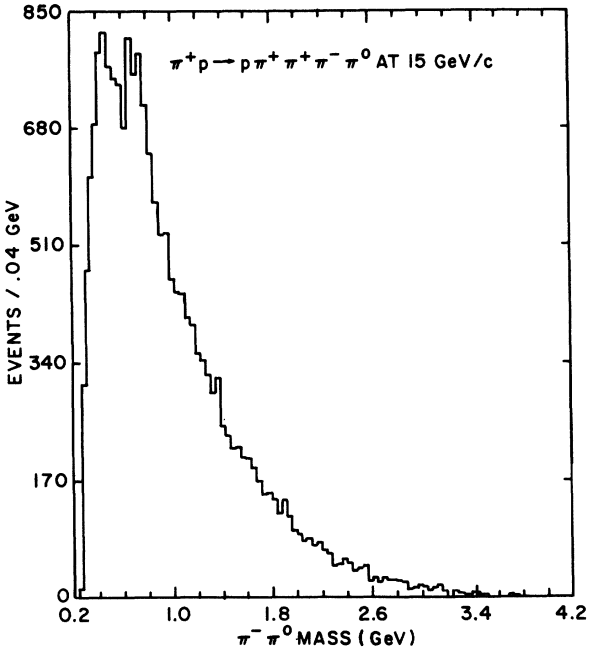

FIG. 8. $\pi^-\pi^0$ mass distribution from reaction (2).

mesons. The A_2 is also seen in the $\pi^+\pi^+\pi^-$ mass distribution of Fig. 10. Fits to both distributions yielded the following values for the mass and width of the A_2:

$$M = 1320 \pm 10 \text{ MeV}, \quad \Gamma = 110 \pm 15 \text{ MeV}.$$

Cross sections are given in Table V. We note that half the three-pion decays of the A_2^+ are via $\rho^+\pi^0$, which is not seen in reaction (4). All the three-pion decays of the A_2^0 are observed. The $\pi^+\pi^-\pi^0$ system produced opposite Δ^{++} is studied in Ref. 31.

The 4π mass spectrum is shown in Fig. 11. There is an enhancement around 1680 MeV, pos-

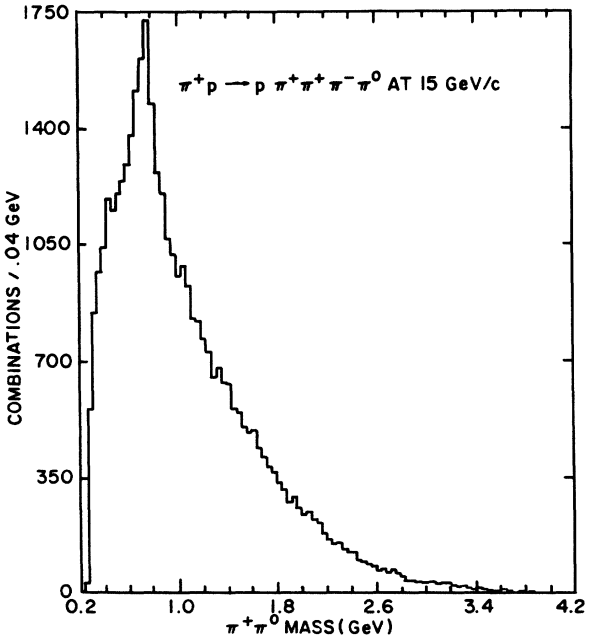

FIG. 7. $\pi^+\pi^0$ mass distribution from reaction (2).

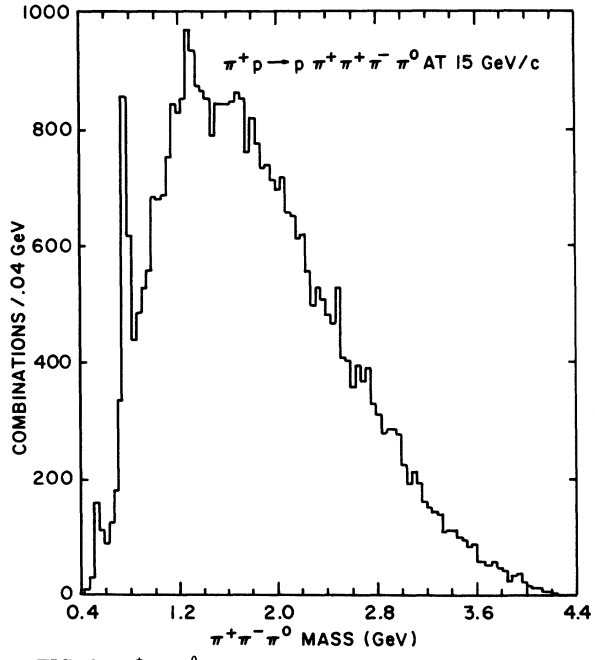

FIG. 9. $\pi^+\pi^-\pi^0$ mass distribution from reaction (2).

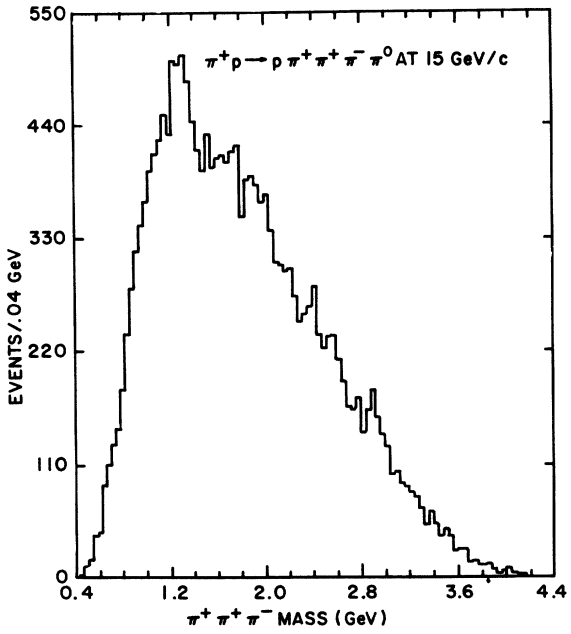

FIG. 10. $\pi^+\pi^+\pi^-$ mass distribution from reaction (2).

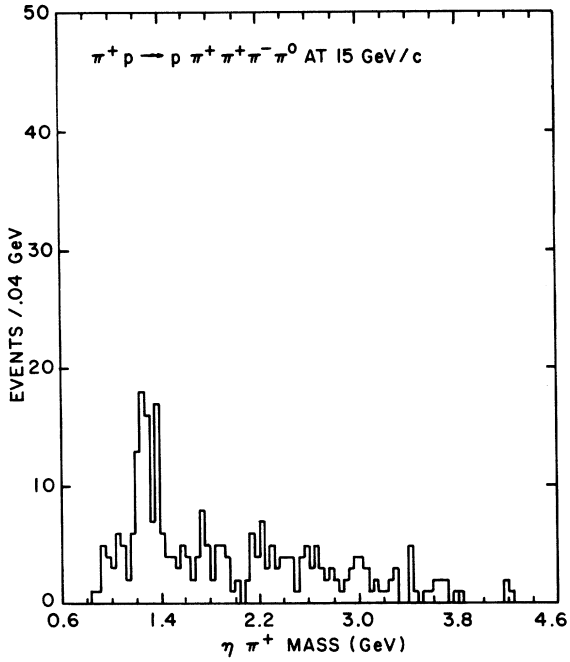

FIG. 12. $\eta\pi^+$ mass distribution from reaction (2).

sibly representing a 4π decay of the g^+ meson. This question is discussed at length in Sec. IV. The enhancement in the 1200–1400-MeV region is primarily the B meson; however, a part of the enhancement is the A_2^+ meson seen in this 4π state through its $\eta\pi^+$ decay, followed by $\eta \rightarrow \pi^+\pi^-\pi^0$. The 4π distribution does not clearly resolve the two resonances. To demonstrate the presence of both resonances, we show the $\eta\pi$ and $\omega\pi$ mass distributions in Figs. 12 and 13, respectively. To determine the cross section for A_2 production, we have fitted the $\eta\pi$ distribution using the same

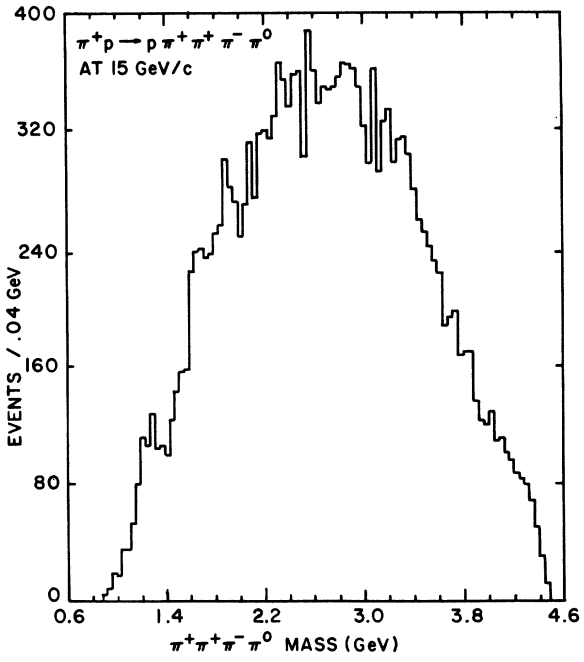

FIG. 11. $\pi^+\pi^+\pi^-\pi^0$ mass distribution from reaction (2).

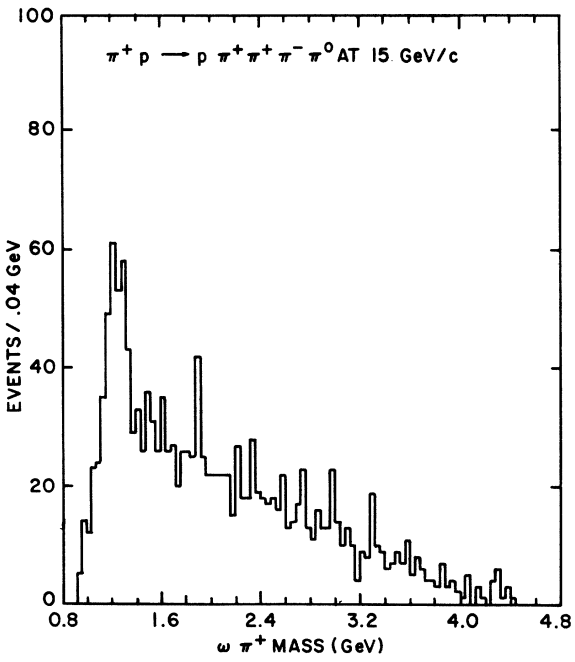

FIG. 13. $\omega\pi^+$ mass distribution from reaction (2).

mass and width parameters as obtained from the best fit to the 3π plots. The cross section given in Table V includes corrections for background under the η and the loss of η events by the 3π mass cut we used.

We have similarly obtained the cross section for $\pi^+p \to pB^+$, followed by $B^+ \to \omega\pi^+$. In fitting the $\omega\pi$ mass plot, we have permitted the B mass and width to vary, obtaining the best fit for the values:

$$M = 1240 \pm 15 \text{ MeV}, \quad \Gamma = 170 \pm 50 \text{ MeV}.$$

The cross section in Table V has been corrected for background under the ω, and loss of events in the ω tail. The background subtractions were made by examining control regions above and below the ω, and fitting to obtain the number of corresponding B events. Details of the background subtraction technique are given in Sec. IV.

3. $\pi^+p \to p3\pi^+2\pi$

A total of 7688 events satisfied our selection criteria for the reaction

$$\pi^+p \to p3\pi^+2\pi^-. \tag{3}$$

Figure 14 shows the $\pi^+\pi^-$ mass distribution, with six combinations per event. The ρ meson is prominent, while the f is seen as a shoulder over the large combinatorial background. There is no evidence for the g meson. The A_2 is the only clear resonance in the $\pi^+\pi^+\pi^-$ and $\pi^+\pi^-\pi^-$ mass distributions, shown in Figs. 15 and 16, respectively.

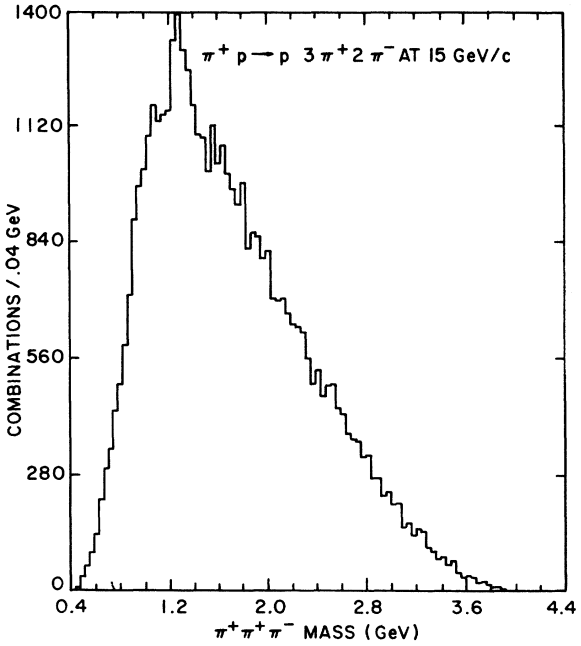

FIG. 15. $\pi^+\pi^+\pi^-$ mass distribution from reaction (3).

Cross sections for these resonances are given in Table V.

Figure 17(a) shows the effective mass of the five pions, requiring that two distinct $\pi^+\pi^-$ mass combinations lie in the ρ^0 mass region (620–920 MeV). There were 4632 events which satisfied this re-

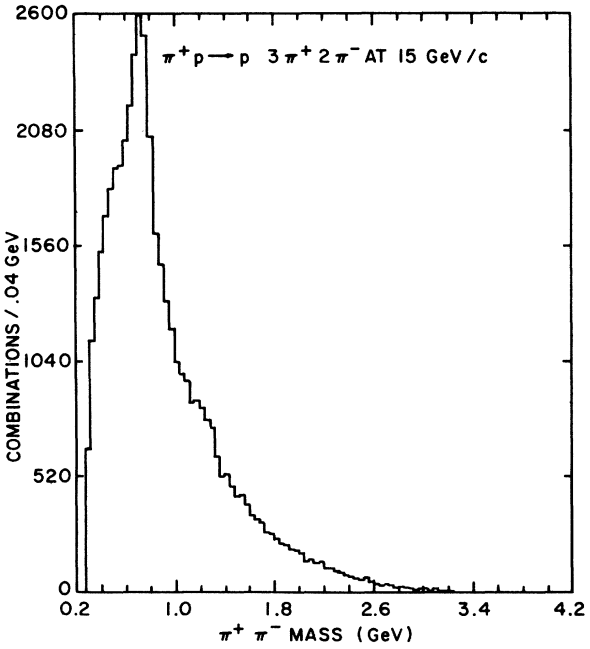

FIG. 14. $\pi^+\pi^-$ mass distribution from reaction (3).

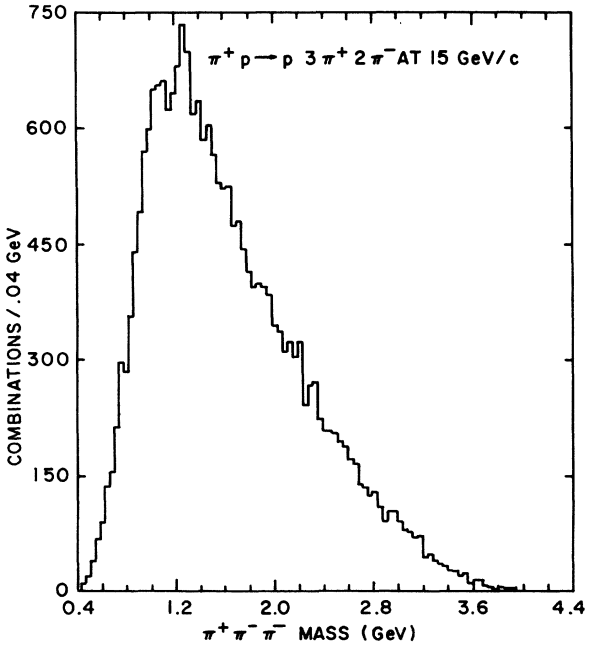

FIG. 16. $\pi^+\pi^-\pi^-$ mass distribution from reaction (3).

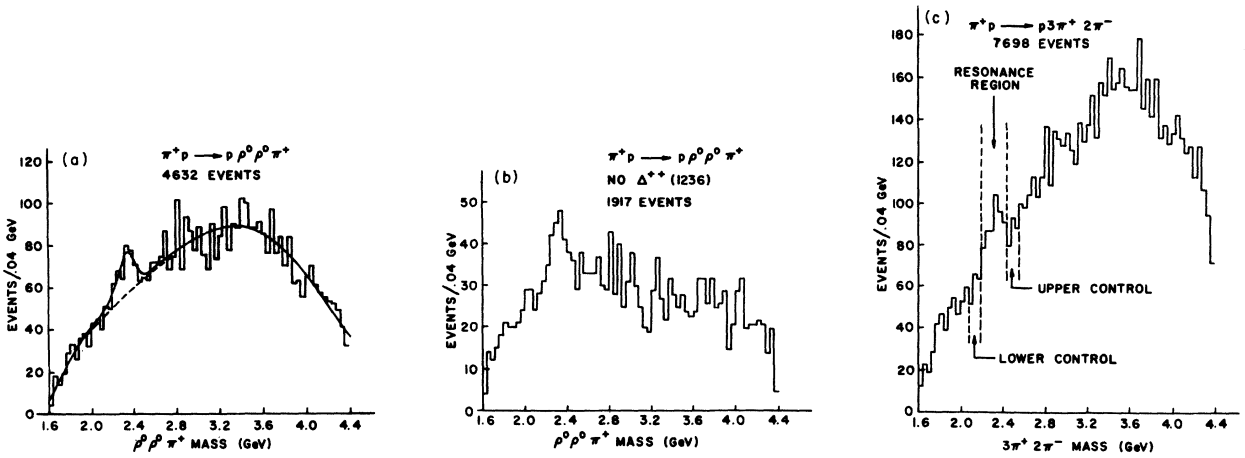

FIG. 17. (a) $\rho^0\rho^0\pi^+$ mass distribution from reaction (3). The curve represents a Breit-Wigner fit plus a polynomial. (b) $\rho^0\rho^0\pi^+$ mass distribution from reaction (3), removing all events with any $p\pi^+$ mass combination below 1360 MeV. (c) The uncut $3\pi^+2\pi^-$ mass distribution from reaction (3).

quirement. In the vicinity of 2340 MeV, the $\rho^0\rho^0\pi^+$ mass distribution shows a 4.5-standard-deviation enhancement above a low-order polynomial fit to the data.[3] The $\rho\rho\pi$ mass resolution (σ) at 2340 MeV is ~15 MeV.

We have performed a fit of the $\rho\rho\pi$ mass distribution to a polynomial background and a Breit-Wigner resonance shape for the enhancement. The best fit, which had a χ^2 of 55 for 63 degrees of freedom is indicated by the solid line in Fig. 17(a) and the background is represented by the dotted line. This fit yielded the following resonance parameters: $M = 2340 \pm 20$ MeV, $\Gamma = 180 \pm 60$ MeV. There were a total of 126 ± 28 events in the resonance, corresponding to a production cross section of 7.3 ± 1.7 μb.

Reaction (3) is characterized by copious production of the $\Delta^{++}(1236)$ resonance. Figure 17(b) shows the $\rho^0\rho^0\pi^+$ mass distribution, removing all events with any $p\pi^+$ mass combination less than 1360 MeV. The mass plot still shows a clear signal for the 2340-MeV resonance, indicating that the effect is not a kinematical reflection of the Δ.

In view of the large background under the ρ meson, it is not clear from the $\rho\rho\pi$ mass plot alone that the resonant events truly represent a $\rho\rho\pi$ state. We have attempted to measure the $\rho\rho\pi$ branching ratio by the following technique. In Fig. 17(c), which shows the uncut 5π mass distribution from reaction (3), we have defined a resonance region and a control band on either side. We have also performed a fit of this distribution using the same mass and width values for the resonance as obtained from the best fit of the $\rho\rho\pi$ plot. The fit yielded the numbers of resonant and background events in the signal and control regions of 5π mass. For events in the resonance region of 5π mass, we have made a scatter plot of one $\pi^+\pi^-$ mass combination against a different $\pi^+\pi^-$ combination from the same event. There are six entries for each event. We have drawn the two ρ bands on the scatter plot and counted the number of events in the overlap box. From the overlap region, we have subtracted events corresponding to background boxes around the overlap, and corrected for the tail of the ρ to obtain the number of true $\rho\rho\pi$ events when the 5π mass is in the resonance region. To make the subtraction of $\rho\rho\pi$ events due to the nonresonant background in the resonance region of 5π mass, we have used the control regions below and above the resonance. We have made similar scatter plots to obtain the number of true $\rho\rho\pi$ events when the 5π mass is in the control regions. Then, assuming that the amount of $\rho\rho\pi$ from the nonresonant background varies smoothly between the two control regions, a subtraction was made, taking into account the fact that the tails of the 2340-MeV resonance extend into the control regions.

We obtain strikingly different numbers for the $\rho\rho\pi$ branching ratios of the 2340-MeV resonance and the background events. For the resonance, we get a branching ratio of 1.05 ± 0.25 into $\rho\rho\pi$ while for the background, we get 0.16 ± 0.04. Our data therefore indicate a dominant $\rho\rho\pi$ decay for the resonance.

With a dominant $\rho\rho\pi$ decay, we would expect, in addition to $\rho^0\rho^0\pi^+$, decays into $\rho^+\rho^0\pi^0$, $\rho^+\rho^+\pi^-$, and $\rho^+\rho^-\pi^+$. All three of the latter decays lead to a $p\pi^+\pi^+\pi^-\pi^0\pi^0$ final state, which is kinematically unfittable, and thus the 5π effective mass cannot be calculated. We have, however, examined the distribution of the missing mass opposite the proton

in events which are consistent with $p\pi^+\pi^+\pi^-$ and two or more missing π^0's. We find a bump near 2340 MeV with a statistical significance of about three standard deviations. This bump is independent evidence for the existence of a resonance at 2340 MeV. It contains 480 ± 200 events above background when fitted by a Breit-Wigner shape centered at 2340 MeV with a width of 180 MeV, which is about 4 times the number of events in the $\rho^0\rho^0\pi^+$ peak of Fig. 17(a). This ratio is in principle sensitive to the isotopic spin of the 2340-MeV resonance; however, because of the large errors on the number of events in the peak in the missing-mass distribution (480 ± 200) and the complexity of the $\rho\rho\pi$ system, we can draw no conclusions.

We have examined our data further to see if the $\rho\rho\pi$ state is the decay of an $A_2\rho$ intermediate state. We have used the same technique as for the determination of the $\rho\rho\pi$ branching ratio, this time making a scatter plot of $\pi^+\pi^-$ mass against $\pi^+\pi^+\pi^-$ mass. Our analysis yields a branching ratio of 0.19 ± 0.27 into $A_2\rho$. We therefore do not have any clear evidence for an $A_2\rho$ decay mode.

We have also searched for 3π and 7π decay modes of this resonance, by examining the four- and eight-prong reactions (1) and (5).

We do not see an enhancement at 2340 MeV in either the 3π or the 7π mass distribution from reactions (1) and (5), respectively. To place an upper limit on the relative rates, we fitted a polynomial to the mass plots and counted the number of events above the fit in a 240-MeV-wide interval around the resonance mass. To this number of possible resonant events, we added one standard deviation on the total number of events in the resonance region to obtain upper limits at the 68% confidence level. We obtained an upper limit of 9% for the 3π decay and 8% for the 7π decay. We also calculated an upper limit of 3% on the branching ratio for the $f^0\pi^+\pi^+\pi^-$ decay.

The observation of a charged state for the resonance implies that the isospin is at least 1. An upper limit of 2 can be placed on the isospin by observing that the initial π^+p state is a pure state of isospin $\frac{3}{2}$, and the resonance is produced with a proton in the final state. The G parity is odd, since the state decays into an odd number of pions.

We have studied the t' dependence of the production cross section for the resonance. t' is defined to be $t - t_{min}$, where t is the square of the four-momentum transfer from the target to the outgoing proton, and t_{min} is the minimum value of t kinematically possible for the event under consideration. We have binned the data in t', plotted the $\rho\rho\pi$ mass separately for each t' bin, and fitted by a Breit-Wigner shape to determine the number of resonant events in each t' bin. Figure 18 shows

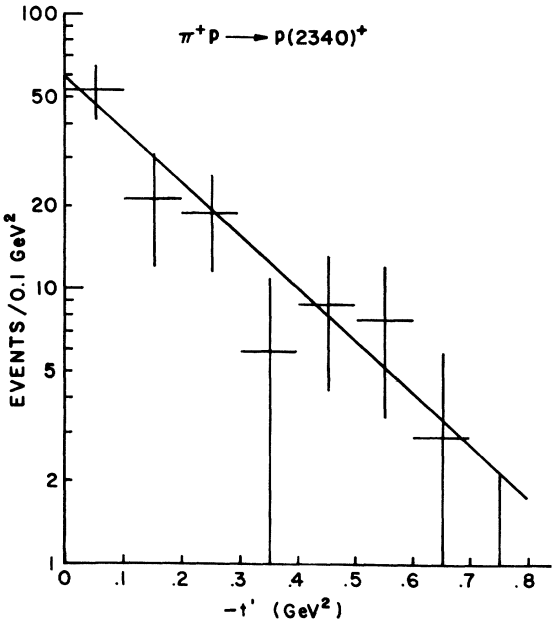

FIG. 18. The t' distribution for the (2340) resonance.

the t' distribution. We have fitted the distribution with the form $\exp(at')$; the results of the best fit are indicated by the solid line in the figure, with a slope parameter of $a = 4.4 \pm 0.9$ GeV^{-2}.

We conclude that we have evidence for a new broad meson resonance at 2340 ± 20 MeV, decaying primarily into $\rho\rho\pi$, with isotopic spin 1 or 2 and odd-G parity. With a mass resolution of 15 MeV in this region, we find the width of the resonance to be 180 ± 60 MeV. The production of the resonance in reaction (3) does not seem to be diffractive as indicated by the slope of the t' distribution. This resonance may be connected with an $I = 1$ enhancement in the nucleon-antinucleon total cross section observed by Abrams *et al.*[29] at a mass of 2350 ± 10 MeV with a width of 140 MeV. However, we feel that this resonance is not related to the so-called U meson that has been reported in missing-mass experiments[30] since the large width observed here is not compatible with the very small (<30 MeV) width reported for the U meson.

4. $\pi^+p \to p3\pi^+2\pi^-\pi^0$

A total of 11316 events satisfied our selection criteria for the reaction

$$\pi^+p \to p3\pi^+2\pi^-\pi^0. \tag{4}$$

Figures 19–21 show the $\pi^+\pi^-$, $\pi^+\pi^0$, and $\pi^-\pi^0$ mass distributions. Only the ρ meson is prominent in these plots. Cross sections are given in Table V. In the charged-3π plots of Figs. 22 and 23, there is only a weak enhancement in the A_2 region. We

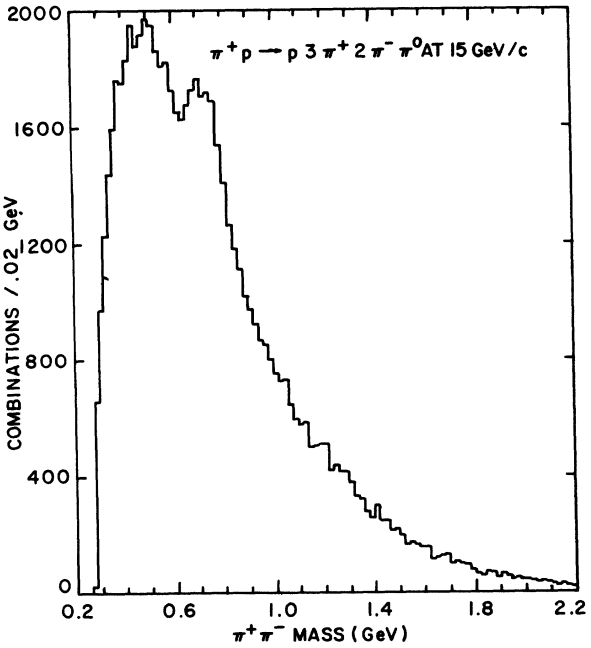

FIG. 19. $\pi^+\pi^-$ mass distribution from reaction (4).

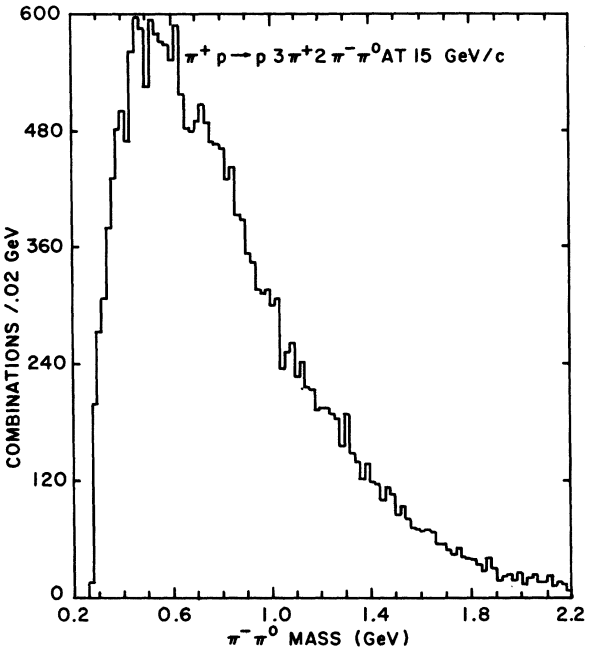

FIG. 21. $\pi^-\pi^0$ mass distribution from reaction (4).

have fitted the distributions in an effort to estimate the cross section, using mass and width values for the A_2 obtained previously. The $\pi^+\pi^-\pi^0$ mass distribution, shown in Fig. 24, exhibits more structure, with the η and ω providing clear signals. The A_2 is possibly present also.

We have examined the other multipion mass distributions without observing convincing evidence for resonance production.

5. $\pi^+ p \rightarrow$ eight charged prongs

In the eight-prong and higher topologies, the combinatorial background is very large and we generally do not observe resonance signals. The

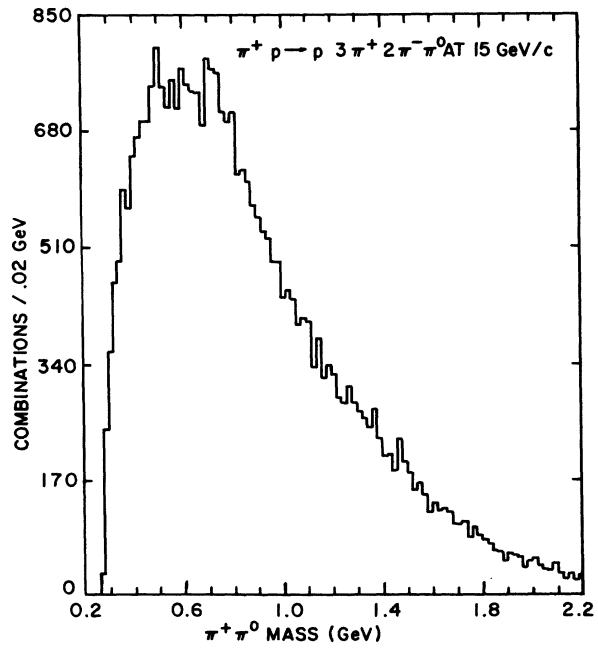

FIG. 20. $\pi^+\pi^0$ mass distribution from reaction (4).

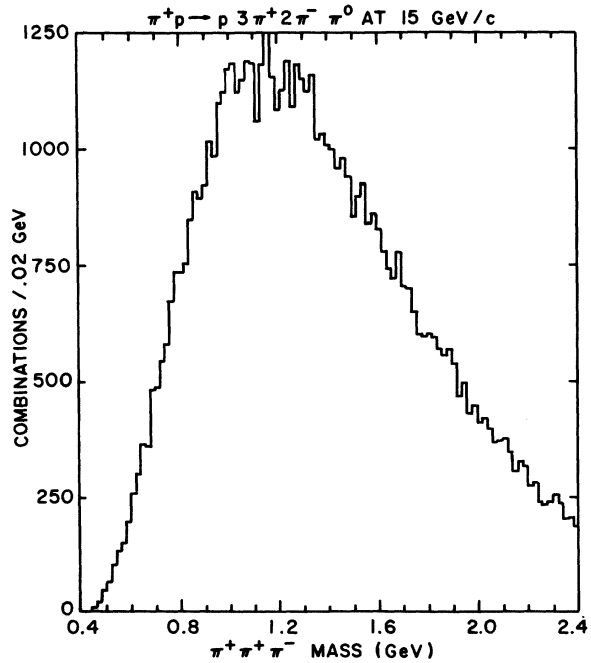

FIG. 22. $\pi^+\pi^+\pi^-$ mass distribution from reaction (4).

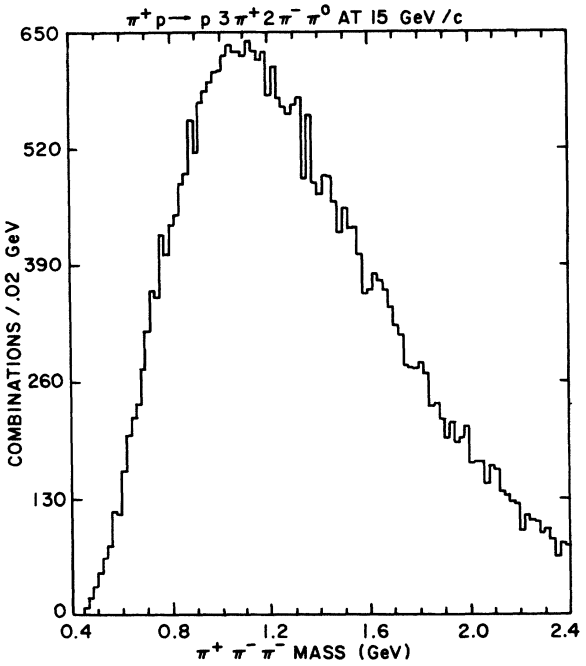

FIG. 23. $\pi^+\pi^-\pi^-$ mass distribution from reaction (4).

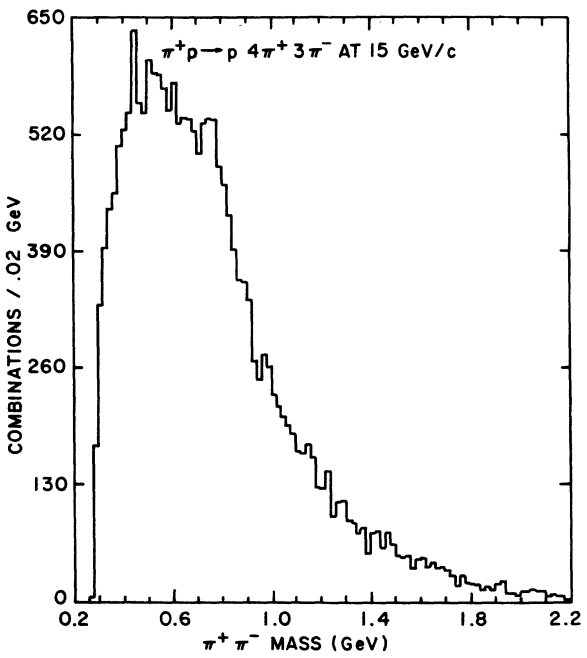

FIG. 25. $\pi^+\pi^-$ mass distribution from reaction (5).

ρ meson is seen in the $\pi^+\pi^-$ mass distribution of Fig. 25, which is derived from 1733 events satisfying our selection criteria for the reaction

$$\pi^+ p \rightarrow p 4\pi^+ 3\pi^-. \tag{5}$$

In Figs. 26–28, we show the three dipion masses from 2440 events satisfying our selection criteria for the reaction

$$\pi^+ p \rightarrow p 4\pi^+ 3\pi^- \pi^0. \tag{6}$$

Cross sections for ρ production are given in Table

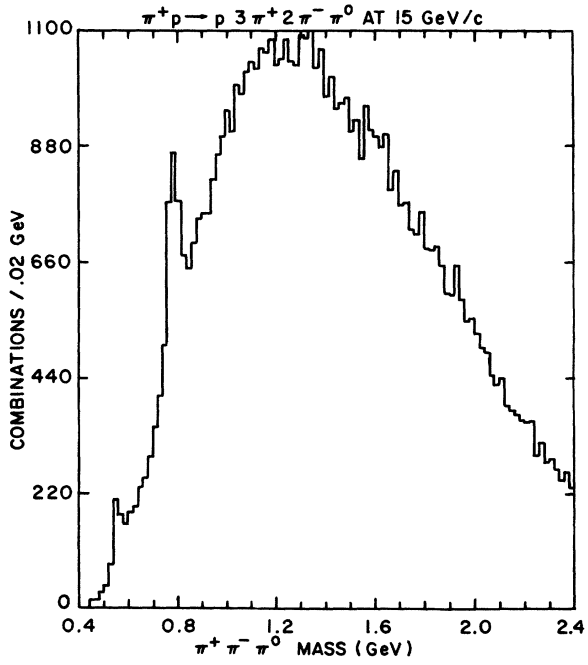

FIG. 24. $\pi^+\pi^-\pi^0$ mass distribution from reaction (4).

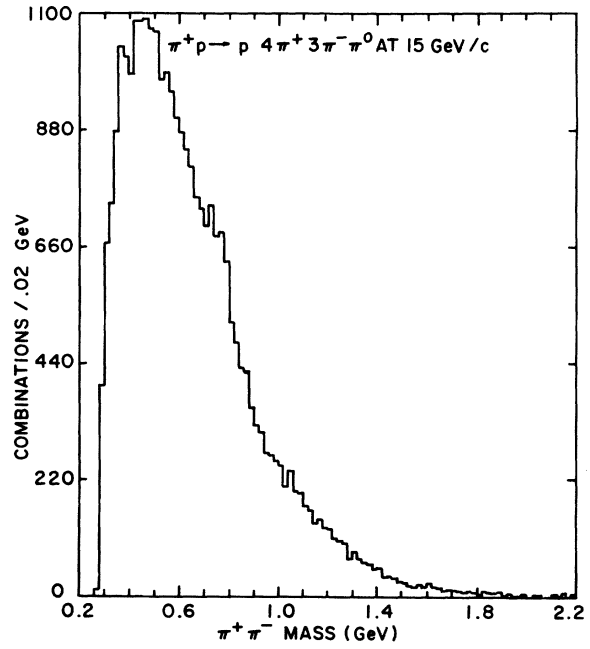

FIG. 26. $\pi^+\pi^-$ mass distribution from reaction (6).

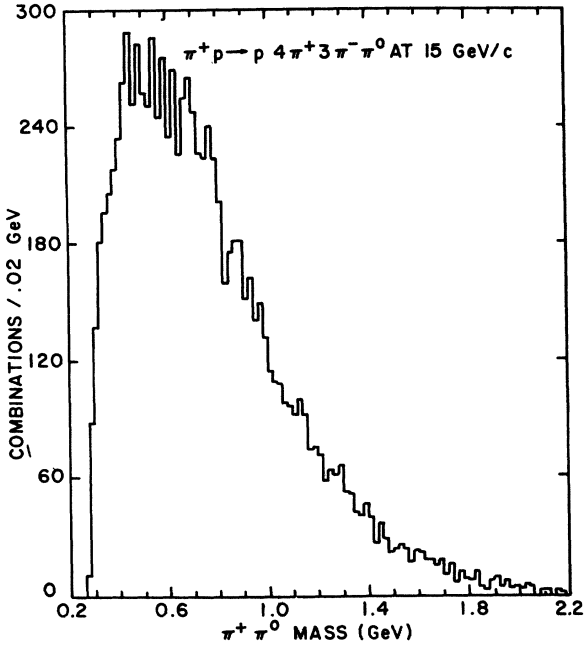

FIG. 27. $\pi^+ \pi^0$ mass distribution from reaction (6).

V.

We have used the multipion mass distributions from reactions (5) and (6) to search for high-mass states that have been reported previously. Results of our search are presented in Sec. V of this paper.

6. $\pi^+ p \rightarrow pMM^+$ and $\pi^+ p \rightarrow p\pi^+ MM^0$

In order to look for resonance production in final states that are kinematically unfittable, we have examined the missing mass recoiling from an identified proton. Figure 29 shows the missing mass, with all topologies included. There are over 200 000 events in the plot. This is an inclusive search for resonance production, since all possible decay modes are represented. We observe a broad enhancement in the region of the A_1 and A_2 mesons, and a smaller signal in the R region, where the A_3 and g mesons lie. Above this region we see a number of bumps, but these are not statistically significant. We note that any resonances in this distribution have a charge of +1 and an isospin equal to 1 or 2.

Figure 30 shows the neutral missing mass in two-prong events with an identified proton. To reduce background, we have eliminated all events that make the elastic 4C fit. The distribution is sensitive to resonances having all neutral decays. We observe convincing signals only for the η and f mesons. A fit to the distribution in the region of the f yields a cross section of 104 ± 17 μb for production of the f in the reaction $\pi^+ p \rightarrow p\pi f^0$, $f^0 \rightarrow$ all neutrals. (The cross section includes a correction for the requirement of an identified proton.) Our measurement of the cross section for $\pi^+ p \rightarrow p\pi f^0$, $f^0 \rightarrow \pi^+ \pi^-$ (see Table V) yielded 216 ± 23 μb. This is

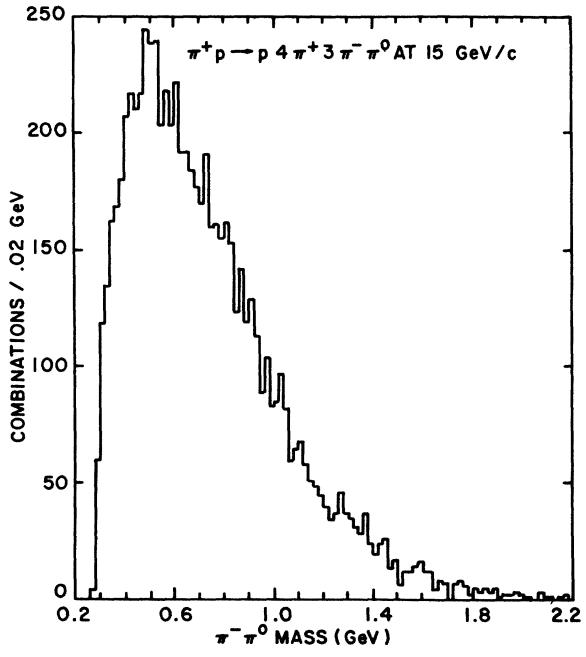

FIG. 28. $\pi^- \pi^0$ mass distribution from reaction (6).

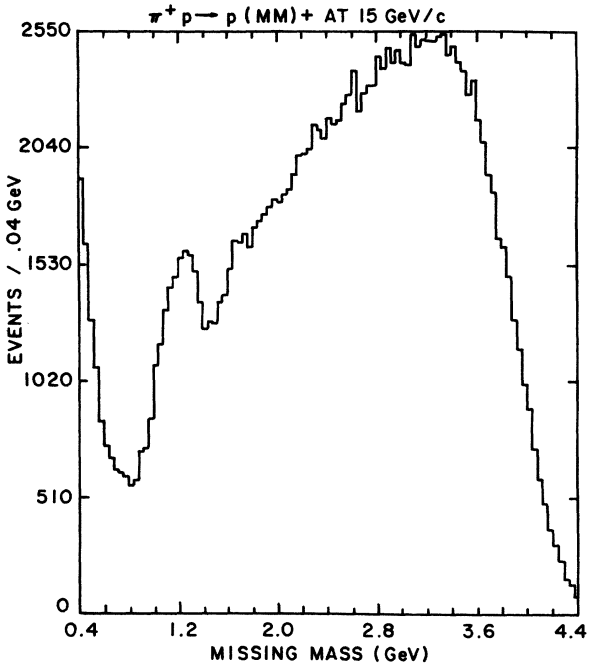

FIG. 29. Distribution of missing mass recoiling from an identified proton for events of all topologies.

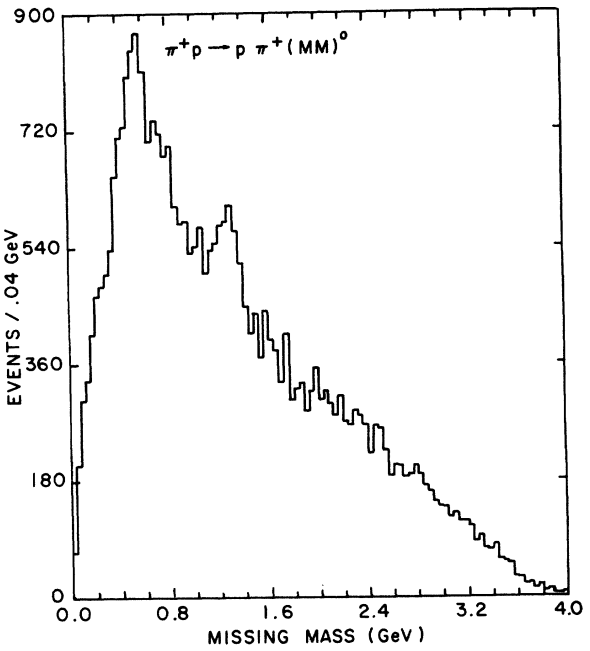

FIG. 30. Distribution of neutral missing mass recoiling from $p\pi^+$ for two-prong events with an identified proton. Elastic events are excluded.

consistent with the expected ratio of $f^0 \to \pi^+\pi^-/f^0 \to \pi^0\pi^0 = 2$ for an isospin-0 resonance.[19]

In Fig. 31 we show the same distribution as Fig. 30 with the further requirement that the $p\pi^+$ mass

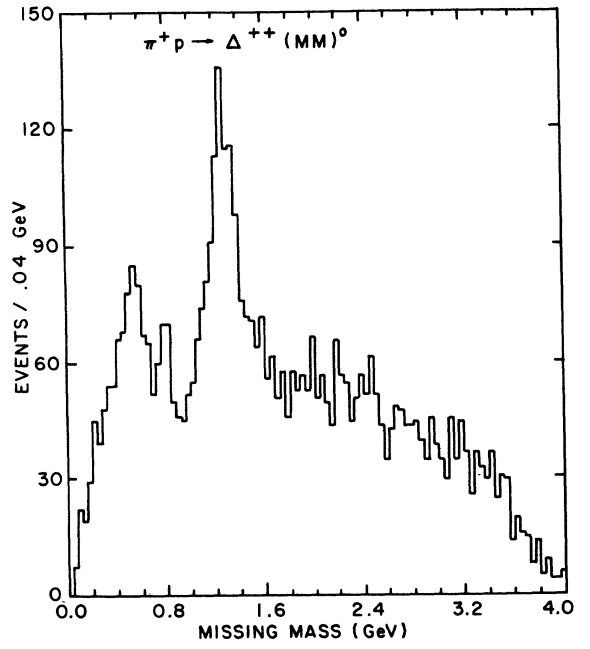

FIG. 31. Distribution of neutral missing mass recoiling from Δ^{++} for two-prong events with an identified proton.

lie in the Δ^{++} region. Resonances in this distribution are in quasi-two-body final states. We observe greatly enhanced signals for the η and f, and possibly also see the $\omega^0 \to \pi^0\gamma$ decay.

IV. BRANCHING RATIOS OF THE g MESON

There have been many studies of the g meson, but the reported results have not been entirely consistent.[19] It is not even clear if there is one or more even-G-parity states in the region around 1680 MeV. Measurements of the branching ratios of the g meson have yielded especially contradictory results.

We have made a study of the neutral g meson, primarily from the four-prong 4C reaction

$$\pi^+ p \to p\pi^+\pi^+\pi^- . \tag{1}$$

Figure 4 shows the $\pi^+\pi^-$ effective mass from reaction (1). In the previous section, we described our method of fitting the ρ, f, and g mesons in this distribution. For the g, we obtained the following parameters:

$$M = 1679 \pm 11 \text{ MeV}, \quad \Gamma = 116 \pm 30 \text{ MeV}.$$

There were 476 ± 120 events in the resonance. We note that the $\pi^+\pi^-$ mass distribution does not show any evidence for more than one resonance in the g region. The mass resolution is 15 MeV. The cross section for g^0 production in reaction (1) is calculated to be 20.7 ± 5.4 μb.

We have measured the ratio of $g^0 \to 2\pi$ to $g^0 \to 4\pi$. We note that $\pi^+\pi^-$ is the only possible 2π decay mode of the g^0. There are only two possible 4π decay modes: $2\pi^+2\pi^-$ and $\pi^+\pi^-2\pi^0$. We have measured the $2\pi^+2\pi^-$ mode by examining events corresponding to the six-prong 4C reaction

$$\pi^+ p \to p 3\pi^+ 2\pi^- . \tag{3}$$

The $2\pi^+2\pi^-$ mass distribution from this reaction shows a weak enhancement in the g region. We have performed a fit to the distribution using parameters for the g^0 as obtained from the best fit to the $\pi^+\pi^-$ plot. The fit yielded a total of 196 ± 70 events in the resonance, corresponding to a cross section of 10.1 ± 3.6 μb for g^0 production in reaction (3).

The other 4π decay mode of the g^0 is $\pi^+\pi^-2\pi^0$, which results in a kinematically unfittable state. We have measured this decay mode by examining all our four-prong events that do not make 4C fits and plotting the neutral missing mass recoiling from the $p\pi^+$ system. From a fit to this distribution we obtained a total of 694 ± 150 events in the resonance, corresponding to a cross section of 59.9 ± 3.1 μb for the reaction

$$\pi^+ p \to p\pi^+ g^0, \quad g^0 \to \pi^+\pi^- 2\pi^0 .$$

TABLE VI. Branching ratios of the g meson.

$(g^+ \to \omega^0 \pi^+)/(g^+ \to \pi^+\pi^+\pi^-\pi^0)$	< 0.11	95% C.L.
$(g^+ \to A_2^+ \pi^0)/(g^+ \to \pi^+\pi^+\pi^-\pi^0)$	0.21 ± 0.06	
$(g^+ \to A_2^0 \pi^+)/(g^+ \to \pi^+\pi^+\pi^-\pi^0)$	0.45 ± 0.06	
$(g^+ \to A_2^{+,0} \pi^{0,+})/(g^+ \to \pi^+\pi^+\pi^-\pi^0)$	0.66 ± 0.08	
$(g^+ \to \rho^+\rho^0)/(g^+ \to \pi^+\pi^+\pi^-\pi^0)$	0.12 ± 0.11	
$(g^+ \to \rho^0\pi^+\pi^0)/(g^+ \to \pi^+\pi^+\pi^-\pi^0)$	0.44 ± 0.08	Incl. $\rho^+\rho^0$
$(g^+ \to \rho^+\pi^+\pi^-/(g^+ \to \pi^+\pi^+\pi^-\pi^0)$	0.47 ± 0.09	Incl. $\rho^+\rho^0$
$(g^+ \to \rho^-\pi^+\pi^+)/(g^+ \to \pi^+\pi^+\pi^-\pi^0)$	0.29 ± 0.07	
$(g^+ \to \rho\pi\pi)/(g^+ \to \pi^+\pi^+\pi^-\pi^0)$	1.08 ± 0.18	Incl. $\rho^+\rho^0$
	0.96 ± 0.21	Excl. $\rho^+\rho^0$
$(g^0 \to 2\pi)/(g^0 \to \text{all } 4\pi)$	0.30 ± 0.10	
$(g^0 \to 3\pi^+3\pi^-)/(g^0 \to 2\pi + g^0 \to 4\pi)$	< 0.01	95% C.L.
$(g^0 \to 2\pi^+2\pi^-2\pi^0)/(g^0 \to 2\pi + g^0 \to 4\pi)$	< 0.05	95% C.L.

This assumes that there is no contribution from decay modes like $\pi^+\pi^-4\pi^0$; $\pi^+\pi^-6\pi^0$, etc. With this assumption, the total $g^0 \to 4\pi$ cross section is found to be 70.0 ± 13.6 μb. The 2π-to-4π ratio is

$$\frac{\sigma(g^0 \to 2\pi)}{\sigma(g^0 \to 4\pi)} = 0.30 \pm 0.10.$$

We have also made a search for possible 6π decays of the g^0. We have examined the $3\pi^+3\pi^-$ mass distribution from events corresponding to the eight-prong 4C reaction

$$\pi^+ p \to p 4\pi^+ 3\pi^-. \tag{5}$$

We observe no enhancement at the g mass. To place an upper limit on the cross section, we have used two standard deviations on the total number of events in a 120-MeV wide interval centered on the g mass. We obtain a 95% confidence level upper limit of 0.8 μb for g^0 production in reaction (5).

To check for the decay into $2\pi^+2\pi^-2\pi^0$, we have studied the missing mass for $p\pi^+$ using all our six-prong events not making 4C fits. The missing mass corresponds to $2\pi^+2\pi^-(n\pi^0)$. We find no evidence for the g, and place a 95% confidence level upper limit of 4.4 μb.

The remaining 6π decay mode is $\pi^+\pi^-4\pi^0$. We cannot distinguish this from the 4π mode $\pi^+\pi^-2\pi^0$. Our upper limits on the 6π branching ratios are given in Table VI.

We have also looked for the charged g meson produced in the reaction $\pi^+ p \to p\pi^+\pi^+\pi^-\pi^0$. In the previous section, it was noted that the effective mass distribution of the four pions (see Fig. 11) showed an enhancement near 1700 MeV which we attribute to the g. We have performed a fit to the distribution, using a second-order polynomial background and a Breit-Wigner shape for the g. The best fit, which had a χ^2 of 42 for 38 degrees of freedom, yielded the following parameters for the g:

$$M = 1665 \pm 15 \text{ MeV}, \quad \Gamma = 105 \pm 30 \text{ MeV}.$$

There were 177 ± 40 events in the resonances. We note that the distribution does not show any evidence for more than one resonance in the g region, where the mass resolution is 15 MeV. We also note that the mass and width are quite consistent with the values obtained from the $\pi^+\pi^-$ decay of the g^0. We therefore tentatively identify the 4π enhancement in reaction (2) as the g^+ meson. The cross section for pg^+ production in reaction (2) is found to be 9.1 ± 2.6 μb.

We have performed a measurement of the branching ratios of the g^+. The experiment of Bartsch *et al.*[20] has found no evidence for an $\omega\pi$ decay, while Thompson *et al.* have reported[21] a branching ratio as high as 0.33 ± 0.07. In Fig. 13 we show the $\pi^+\pi^+\pi^-\pi^0$ mass distribution, requiring the $\pi^+\pi^-\pi^0$ mass to lie in the ω region (740–840 MeV). We observe a strong signal for the B meson, but no indication of the g. A fit to the distribution, using parameters obtained from our best fit to the uncut 4π mass, yielded no events for the g. To place an upper limit on the $\omega\pi$ branching ratio, we have taken two standard deviations on the total number of events in a 120-MeV wide interval centered on the g mass. We obtain

$$\frac{\sigma(g^+ \to \omega\pi^+)}{\sigma(g^+ \to \pi^+\pi^+\pi^-\pi^0)} < 0.11, \quad 95\% \text{ C.L.}$$

We also find no evidence for an $\omega\pi$ decay of the g when we compare the amount of ω's produced

in the g region with ω production in control regions above and below the g.

The $A_2\pi$ and $\rho\rho$ decays of the g present a confusing situation. A dominant $A_2\pi$ decay has been reported by one group,[22] while others have found a dominant $\rho\rho$ mode.[23] Thompson *et al.* have measured a branching ratio of 0.36 ± 0.14 into $A_2\pi$ and 0.13 ± 0.09 into $\rho\rho$.[21] They have pointed out that a large fraction of 4π phase space in the g region falls within ρ mass cuts, and there is a large overlap of $\rho\rho$ and $A_2\pi$ channels. Not all experiments have attempted background subtractions, and comparisons are therefore difficult to make.

To determine the $A_2\pi$ branching ratio, we first examined the uncut $\pi^+\pi^+\pi^-$ and $\pi^+\pi^-\pi^0$ mass spectra, and fitted them to background polynomials plus Breit-Wigner shapes for the A_2. The results of these fits were described in the previous section. Next, in the uncut 4π mass plot we defined a resonance region from 1.60 to 1.76 GeV and an 80-MeV-wide control band on either side. For events in the resonance region, we plotted the $\pi^+\pi^+\pi^-$ and $\pi^+\pi^-\pi^0$ mass subsets and performed fits to the A_2 using the parameters from the best fits to the uncut 3π plots. This procedure gave us the number of A_2^+ and A_2^0 events when the 4π mass is in the resonance region. To make the subtraction of A_2 events due to the nonresonant background in the resonance region of 4π mass, we then used the control regions below and above the g. We fit similar 3π mass distributions to obtain the number of A_2^+ and A_2^0 events when the 4π mass is in the control regions. Then, assuming that the amount of A_2 from the nonresonant background varies smoothly between the two control regions, a subtraction was made, taking into account the fact that the tails of the g extend into the control regions. Our results are given in Table VI. We note that since the $A_2^+ \to \rho^+\pi^0$ decay is not detected, the branching ratio for $g^+ \to A_2^0\pi^+$ is expected to be twice that for $g^+ \to A_2^+\pi^0$. Our results are in excellent agreement with this prediction. The total $A_2\pi$ branching ratio is found to be

$$\frac{\sigma(g^+ \to A_2\pi)}{\sigma(g^+ \to \pi^+\pi^+\pi^-\pi^0)} = 0.66 \pm 0.08.$$

We have used a similar technique to measure the $\rho^+\rho^0$ branching ratio. From the resonance and control regions of 4π mass, we have made scatter plots of $\pi^+\pi^0$ mass versus $\pi^+\pi^-$ mass. We have drawn the two ρ bands on each scatter plot and counted the number of events in the overlap box. From the overlap region, we have subtracted events corresponding to background boxes around the overlap, and corrected for the tail of the ρ to obtain the number of true $\rho\rho$ events when the 4π mass is in a particular region. The background subtraction was performed as for the A_2, assuming that the amount of $\rho\rho$ from the nonresonant background varies smoothly between the control regions. Our result is that

$$\frac{\sigma(g^+ \to \rho^+\rho^0)}{\sigma(g^+ \to \pi^+\pi^+\pi^-\pi^0)} = 0.12 \pm 0.11.$$

The main contribution to the error is the statistical error on the number of $\rho^+\rho^0$ events from the three regions of 4π mass.

Measurements of the $\rho\pi\pi$ decay mode have generally found[20,24] the branching ratio to be consistent with 1. We have measured the $\rho^0\pi^+\pi^0$, $\rho^+\pi^+\pi^-$, and $\rho^-\pi^+\pi^+$ branching ratios separately by fitting the $\pi^+\pi^-$, $\pi^+\pi^0$, and $\pi^-\pi^0$ mass subsets of 4π mass in resonance and control regions. The background subtraction was performed as described previously for the $A_2\pi$ decay. The results are given in Table VI. The total $\rho\pi\pi$ branching ratio is found to be

$$\frac{\sigma(g^+ \to \rho\pi\pi)}{\sigma(g^+ \to \pi^+\pi^+\pi^-\pi^0)} = \begin{cases} 1.08 \pm 0.18 \text{ including } \rho^+\rho^0, \\ 0.96 \pm 0.21 \text{ excluding } \rho^+\rho^0. \end{cases}$$

V. SEARCH FOR CLAIMED HIGH-MASS RESONANT STATES

In the mass region above 3 GeV, resonances have been claimed in two experiments with fitted final states. One is a 6.94-GeV/c antiproton annihilation experiment of a Tel Aviv group.[25] In the 7π final state, this group searched for resonances in the $3\pi^+3\pi^-$ effective mass. From 1196 events, two enhancements were seen, at 3.08 and 3.39 GeV, respectively.

In an attempt to search for these claimed resonances we have examined the $3\pi^+3\pi^-$ mass from reactions (5) and (6). We observe no evidence for the resonances in either distribution. We can place an upper limit of about 2.5 μb on the production cross section for these claimed enhancements by taking one standard deviation on the total number of entries in a mass range of 0.22 GeV centered at the claimed masses. (0.22 GeV is the claimed width of the states.)

Another observed high-mass state is from a Florida State π^+p bubble-chamber experiment at 11 GeV/c.[26] The experiment is therefore closely comparable to the one reported in this paper. From 171 eight-prong 1C events, corresponding to our reaction (6), the group reported a narrow bump in both the neutral and charged 7π channels at 3.01 GeV.

We have examined our $3\pi^+3\pi^-\pi^0$ and $4\pi^+3\pi^-$ mass distributions from 2440 events corresponding to reaction (6). We have also tried binning the data in a manner identical to that of Ref. 26, as well as imposing the identical cuts on the data, but do not see the claimed signal. We place a one standard

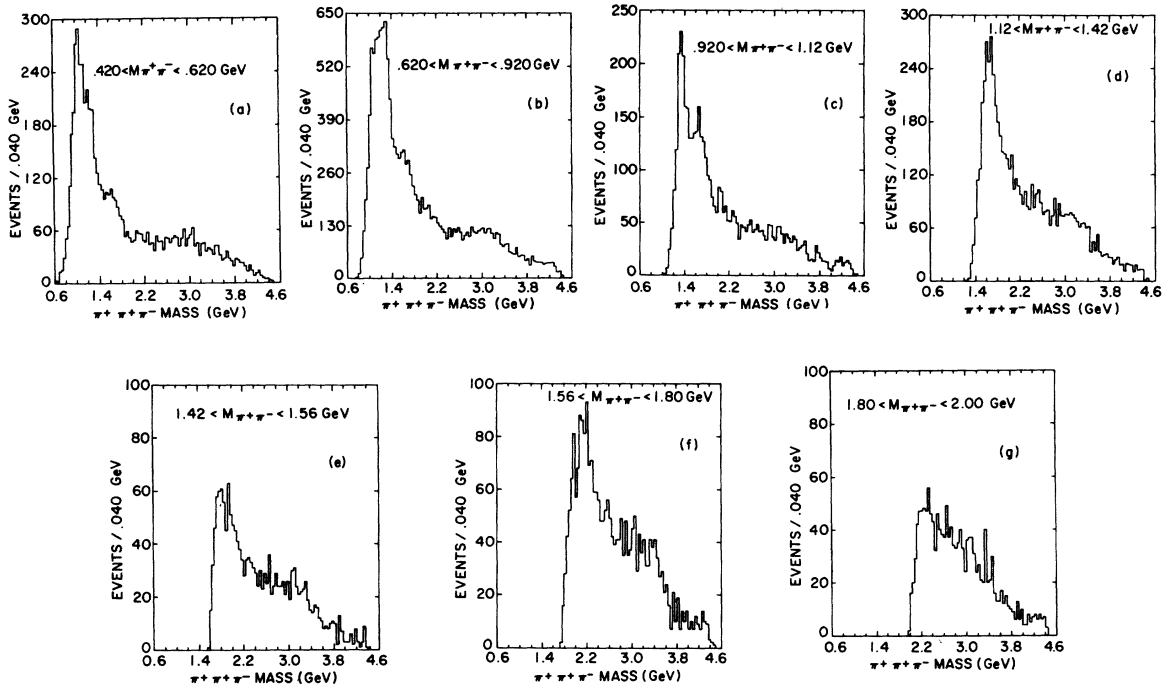

FIG. 32. $\pi^+\pi^+\pi^-$ mass distribution from reaction (1), requiring $\pi^+\pi^-$ mass to lie in the regions shown.

deviation upper limit of about 1.5 μb on the cross section.

VI. THE A MESONS

A. The A_4 meson

Figure 4 shows the $\pi^+\pi^-$ mass distribution from reaction (1). The presence of the ρ, f, and g mesons is apparent in this distribution. Selecting events with a $\pi^+\pi^-$ combination in the ρ, the $\rho^0\pi^+$ mass spectrum, shown in Fig. 32(b), exhibits the well known threshold enhancement near 1100 MeV known as the A_1. The A_2 meson also contributes to the enhancement. Selecting events with a $\pi^+\pi^-$ mass in the f region, the $f^0\pi^+$ mass spectrum of Fig. 32(d) shows the enhancement near 1650 MeV known as the A_3. In a similar way, when we select events with the $\pi^+\pi^-$ mass in the g-meson region, and plot the $g^0\pi^+$ mass spectrum in Fig. 32(f), we observe an enhancement near 2050 MeV, which may naturally be called the A_4. A π-p experiment at 25 GeV/c has reported[27] an A_4 at 2100 MeV.

The interpretation of these A_1, A_3, and A_4 enhancements as resonances or threshold effects is not clear. We have plotted the $\pi^+\pi^+\pi^-$ mass distributions for events where the $\pi^+\pi^-$ mass is in control regions below the ρ, between the ρ and f, between the f and g, and above the g. Figures 32(a),, 32(c), 32(e), and 32(g) show these plots. All of these distributions are characterized by similar low-mass enhancements typically 300 to 400 MeV above the $\pi^+\pi^-$ mass selected. The A_1, A_3, and A_4 effects may therefore at least partly be

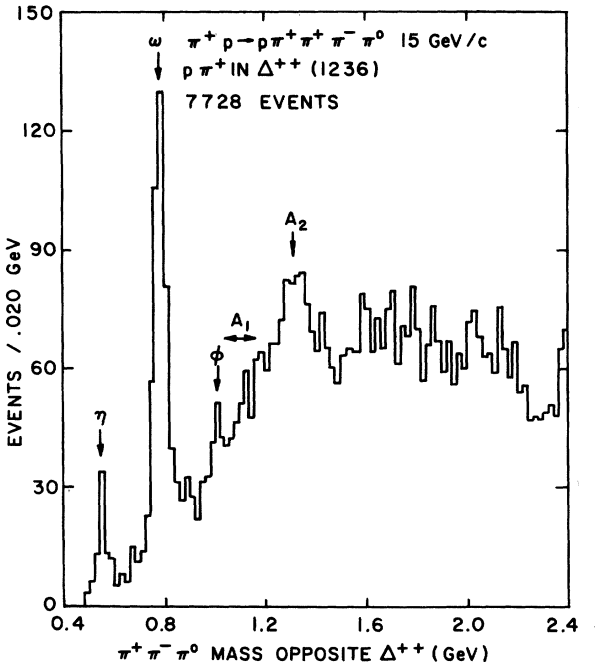

FIG. 33. $\pi^+\pi^-\pi^0$ mass distribution opposite Δ^{++} from reaction (2).

of kinematic origin. A partial-wave analysis of the $\pi^+\pi^+\pi^-$ system confirms this suggestion.[31]

B. Search for nondiffractive A_1 production

Kane has recently reemphasized[28] the importance of the existence of an axial-vector-meson state, and has pointed out that if the A_1 is a resonant state, it should also be produced in nondiffractive channels such as $\pi^+p \to \Delta^{++}A_1$. He has estimated a cross section of 15 μb for this process at 15 GeV/c, with an absolute lower limit of 2 μb.

We have selected 7728 events of reaction (2) with a $p\pi^+$ mass in the Δ^{++} region, corresponding to a sensitivity of 20 events/μb. Figure 33 shows the $\pi^+\pi^-\pi^0$ mass distribution opposite the Δ^{++} from reaction (2). We observe very clear signals for the production of the η, ω, and the A_2^0. However, we see no evidence for the A_1. We can place a one standard deviation upper limit of 1.5 μb on the cross section, for an A_1 width of 150 MeV or less. This limit is less than the cross section expected by Kane, although his 2-μb absolute lower limit is not conclusively ruled out. The nondiffractive production of the A mesons is studied in more detail in Ref. 31 where a tighter upper limit for A_1 production is set.

ACKNOWLEDGMENTS

We would like to thank the Columbia University HPD staff, the scanning departments and computer centers at Columbia and Binghamton, and the operating crew of the 82-in. bubble chamber at SLAC.

---

*Research supported by the National Science Foundation.

†Present address: Argonne National Laboratory, Argonne, Ill. 60439.

‡Present address: University of Washington, Seattle, Wash. 98105.

§Present address: New York University, New York, N. Y. 10003.

[1]C. Baltay *et al.*, Phys. Rev. Lett. 34, 1118 (1975).

[2]C. Baltay *et al.*, Phys. Lett. 57B, 293 (1975).

[3]C. Balaty *et al.*, Phys. Rev. Lett. 35, 891 (1975).

[4]C. Baltay *et al.*, in Proceedings of the Summer Symposium at ANL, 1975 [ANL Report No. ANL-HEP-CP-75-58], p. 289.

[5]M. Kalelkar in *Particles and Fields–1975*, proceedings of the meeting of the Division of Particles and Fields of the APS, Seattle, edited by H. J. Lubatti and P. M. Mockett (Univ. of Washington, Seattle, 1976), p. 269.

[6]C. Baltay *et al.*, Phys. Rev. D 14, 55 (1976).

[7]For experimental details, see M. Kalelkar, Ph. D. thesis, Columbia University, Nevis Report No. 207, 1975 (unpublished).

[8]G. Eckman and P. Miller, LRL Engineering Note, code HD0203, serial M4046, 1968 (unpublished).

[9]S. Flatte and F. Solmitz, SLAC Report No. SLAC-TN-69-7, 1969 (unpublished).

[10]J. Cobb, SLAC Report No. SLAC-TN-71-15, 1971 (unpublished).

[11]See also S. Csorna, Ph.D. thesis, Columbia University. Nevis Report No. 211, 1976 (unpublished).

[12]P. Hough and B. Powell, Nuovo Cimento 16, 1184 (1960).

[13]R. Marr and G. Rabinowitz, in *Methods in Computational Physics* (Academic, New York, 1966).

[14]G. Rabinowitz, in *Proceedings of the International Conference on Programming for Flying Spot Devices, Munich, 1967*, edited by B. W. Powell and P. Seyboth (Max Planck Institute, Munich, Germany, 1967).

[15]See also M. Habibi, Ph.D. thesis, Columbia University, Nevis Report No. 199, 1973 (unpublished).

[16]F. Solmitz, A. Johnson, and T. Day, LRL Alvarez Group, Programming Note P-117, 1966 (unpublished).

[17]O. Dahl *et al.*, LRL Group A Programming Note P-126 (unpublished), 1968.

[18]S. Denisov *et al.*, Phys. Lett. 36B, 415 (1971).

[19]Particle Data Group, Phys. Lett. 50B, 1 (1974).

[20]J. Bartsch *et al.*, Nucl. Phys. B22, 109 (1970).

[21]G. Thompson *et al.*, Nucl. Phys. B69, 220 (1974).

[22]C. Baltay *et al.*, Phys. Rev. Lett. 20, 887 (1968).

[23]N. M. Cason *et al.*, Phys. Rev. D 7, 1971 (1973).

[24]J. Ballam *et al.*, Phys. Rev. D 3, 2606 (1971).

[25]G. Alexander *et al.*, Nucl. Phys. B45, 29 (1972).

[26]G. Yost *et al.*, Phys. Rev. D 3, 642 (1971).

[27]Yu. Antipov *et al.*, Nucl. Phys. B119, 45 (1977).

[28]G. Kane (private communication); see also G. Kane, University of Michigan Report No. UMHE 75-3 (unpublished).

[29]R. J. Abrams *et al.*, Phys. Rev. Lett. 18, 1209 (1967); see Also J. Alspector *et al.*, *ibid.* 30, 511 (1973).

[30]G. Chikovani *et al.*, Phys. Lett. 22, 233 (1966).

[31]C. V Cautis, Ph.D. thesis, Columbia University, Nevis Report No. 221, 1977 (unpublished).